Mineralization of organic matter in boreal lake sediments: Rates, pathways and nature of the fermenting substrates

François Clayer[1], Yves Gélinas[2], André Tessier[3], and Charles Gobeil[4]

[1]Norwegian Institute for Water Research
[2]GEOTOP and Concordia University
[3]INRS-ETE, Université du Québec
[4]INRS-ETE

November 22, 2022

Abstract

The complexity of organic matter (OM) degradation mechanisms represents a significant challenge for developing biogeochemical models to quantify the role of aquatic sediments in the climate system. The common representation of OM by carbohydrates formulated as CHO in models comes with the assumption that its degradation by fermentation produces equimolar amounts of methane (CH) and dissolved inorganic carbon (DIC). To test the validity of this assumption, we modeled using reaction-transport equations vertical profiles of the concentration and isotopic composition (δC) of CH and DIC in the top 25 cm of the sediment column from two lake basins, one whose hypolimnion is perennially oxygenated and one with seasonal anoxia. Our results reveal that methanogenesis only occurs via hydrogenotrophy in both basins. Furthermore, we calculate, from CH and DIC production rates associated with methanogenesis, that the fermenting OM has an average carbon oxidation state (COS) below -0.9. Modeling solute porewater profiles reported in the literature for four other seasonally anoxic lake basins also yields negative COS values. Collectively, the mean (±SD) COS value of -1.4 +- 0.3 for all the seasonally anoxic sites is much lower than the value of zero expected from carbohydrates fermentation. We conclude that carbohydrates do not adequately represent the fermenting OM and that the COS should be included in the formulation of OM fermentation in models applied to lake sediments. This study highlights the need to better characterize the labile OM undergoing mineralization to interpret present-day greenhouse gases cycling and predict its alteration under environmental changes.

Mineralization of organic matter in boreal lake sediments: Rates, pathways and nature of the fermenting substrates

F. Clayer[1,3,*], Y. Gélinas[2,3], A. Tessier[1] and C. Gobeil[1,3]

[1]INRS-ETE, Université du Québec, 490 rue de la Couronne, Québec (QC), Canada G1K 9A9

[2]Concordia University, Department of Chemistry and Biochemistry, 7141 Sherbrooke Street West, Montreal (QC), Canada H4B 1R6.

[3]Geotop, Interuniversity research and training centre in geosciences, 201 Président-Kennedy Ave., Montréal (QC), Canada H2X 3Y7.

Corresponding author: François Clayer (francois.clayer@niva.no); Phone: +47 406 28 963

[*]Current address: Norwegian Institute for Water Research (NIVA), Gaustadalléen 21, 0349 Oslo, Norway

Key Points:

- Methanogenesis is dominated by hydrogenotrophy in the hypolimnetic sediment of the studied oligotrophic boreal lakes.
- Substrates for methanogenesis have a negative carbon oxidation state.
- The carbon oxidation state of the substrate should be included in the formulation of organic matter fermentation in biogeochemical models.

Abstract

The complexity of organic matter (OM) degradation mechanisms represents a significant challenge for developing biogeochemical models to quantify the role of aquatic sediments in the climate system. The common representation of OM by carbohydrates formulated as CH_2O in models comes with the assumption that its degradation by fermentation produces equimolar amounts of methane (CH_4) and dissolved inorganic carbon (DIC). To test the validity of this assumption, we modeled using reaction-transport equations vertical profiles of the concentration and isotopic composition ($\delta^{13}C$) of CH_4 and DIC in the top 25 cm of the sediment column from two lake basins, one whose hypolimnion is perennially oxygenated and one with seasonal anoxia. Our results reveal that methanogenesis only occurs via hydrogenotrophy in both basins. Furthermore, we calculate, from CH_4 and DIC production rates associated with methanogenesis, that the fermenting OM has an average carbon oxidation state (COS) below −0.9. Modeling solute porewater profiles reported in the literature for four other seasonally anoxic lake basins also yields negative COS values. Collectively, the mean (±SD) COS value of -1.4 ± 0.3 for all the seasonally anoxic sites is much lower than the value of zero expected from carbohydrates fermentation. We conclude that carbohydrates do not adequately represent the fermenting OM and that the COS should be included in the formulation of OM fermentation in models applied to lake sediments. This study highlights the need to better characterize the labile OM undergoing mineralization to interpret present-day greenhouse gases cycling and predict its alteration under environmental changes.

Plain Language Summary

Organic matter in aquatic sediments is a complex mixture of mainly uncharacterized molecules and can be converted to greenhouse gases, for example methane and carbon dioxide, which can be released into the atmosphere. In current models, organic matter is represented by carbohydrates whose fermentation in oxygen-depleted sediments produces equal amount of methane and carbon dioxide. In this study, we estimated the production rates of methane and carbon dioxide during fermentation in lake sediments using concentration data and carbon isotopes of these greenhouse gases. Our results show that fermentation in the sediment of the deepest parts of the lake produces more methane than carbon dioxide, and that their relative

production rates vary across sites. Hence, carbohydrates are not well-suited to represent organic matter in current models. We therefore propose a new formulation for organic matter fermentation in aquatic sediments to better quantify greenhouse gases release. A more precise formulation for organic matter fermentation in aquatic sediments is crucial to better quantify current greenhouse gas emissions as well as their fate under global climate change.

1 Introduction

Significant proportions of atmospheric methane (CH_4) and carbon dioxide (CO_2), two powerful greenhouse gases, are thought to originate from freshwater lake sediments (Wuebbles and Hayhoe 2002; Bastviken et al., 2004; Turner et al., 2015), but large uncertainties remain concerning their contribution to the global CO_2 and CH_4 budgets (Saunois et al., 2016). The role of these waterbodies in the global carbon (C) budget has been acknowledged for more than a decade (Cole et al. 2007). Especially in the lake-rich boreal region, lakes are hotspots of CO_2 and CH_4 release (Hastie et al., 2018; Wallin et al., 2018) and intensive sites of terrestrial C processing (Holgerson and Raymond, 2016; Staehr et al., 2012). Using high-resolution satellite imagery, Verpoorter et al. (2014) estimated to about 27 million the number of lakes larger than 0.01 km^2 on Earth and reported that the highest lake concentration and surface area are found in boreal regions. Boreal lakes, which are typically small and shallow, are known to store large amounts of organic C, to warm up quickly, and to develop anoxic hypolimnia in the warm season (Schindler et al., 1996; Sabrekov et al., 2017). Owing to the great abundance of boreal lakes, their sensitivity to climate change and foreseen important role in the global C cycle, there is a need to further develop process-based models to better quantify C processing reactions in these lakes and their alteration under warming (Saunois et al., 2016).

In aquatic environments, CH_4 is mainly produced (methanogenesis) in the sediment along with CO_2 at depths where most electron acceptors (EAs) are depleted (Conrad, 1999; Corbett et al., 2013). During its upward migration to the atmosphere, CH_4 is partly aerobically or anaerobically oxidized to CO_2 (methanotrophy) in the upper strata of the sediments and in the water column (Bastviken et al., 2008; Raghoebarsing et al. 2006; Beal et al. 2009; Ettwig et al. 2010; Egger et al. 2015). The oxidation of organic matter (OM) by EAs such as O_2, NO_3^-, Fe(III), Mn(IV), SO_4^{2-} and humic substances, as well as the partial fermentation of high molecular weight organic matter (HMW OM) into lower molecular weight organic matter (LMW

OM) are also potential sources of CO_2 in the sedimentary environment (Corbett et al., 2015). Predicting fluxes of CH_4 and CO_2 from the aquatic sediments and water column to the atmosphere is challenging considering the various transport processes and chemical and microbially-mediated reactions implicated and the complexity of natural OM which serves as substrate (Natchimuthu et al., 2017).

Process-based geochemical models taking into account both the numerous biogeochemical reactions involving C and transport processes are powerful tools able to interpret present-day sediment, porewater and water-column profiles of C species and offer a great potential to forecast changes in cycling of this element under variable environmental scenarios (Wang and Van Cappellen 1996; Arndt et al., 2013; Paraska et al., 2014; Saunois et al., 2016). Nonetheless, the performance of these models depends on the correct formulation of the OM mineralization reactions, particularly in terms of the metabolizable organic compounds involved. Up to now, carbohydrates, represented as the simple chemical formula CH_2O (or $C_6H_{12}O_6$), whose average carbon oxidation state (COS) is zero, are commonly assumed to be representative of the bulk of metabolizable OM, including the substrates involved in fermentation reactions (e.g., Arndt et al., 2013; Paraska et al., 2014; Arning et al., 2016 and references therein). The capacity of CH_2O to represent adequately the ensemble of labile organic compounds is, nevertheless, becoming increasingly questioned in the literature given the variety and complexity of organic molecules present in the environment (Alperin et al., 1994; Berelson et al., 2005; Jørgensen and Parkes, 2010; Burdige and Komada, 2011; Clayer et al., 2016). Based on the observation that methanogenesis produced CH_4 three times faster than CO_2 in the sediments of a boreal, sporadically anoxic lake basin, Clayer et al. (2018) concluded that the fermenting OM had a markedly negative COS value of −1.9. This COS value corresponds more closely to a mixture of fatty acids and fatty alcohols than to carbohydrates (e.g., CH_2O), which would have yielded equivalent CH_4 and CO_2 production rates. The low COS value of metabolizable OM in the sediment layer where methanogenesis occurred in this lake has been attributed to the nearly complete consumption of the most labile organic components (e.g., carbohydrates, proteins) during its downward transport through the water column and the upper sediment layers, thus leaving only material of lower lability such as fatty acids and fatty alcohols available for methanogenesis. Such interpretation, however, must be validated by investigating other lakes before revising the formulation of the fermenting OM used in diagenetic models in order to

improve model predictions of C cycling, including greenhouse gases production and emission from these environments.

In this study, centimeter-scale vertical porewater profiles of the concentrations and of the stable carbon isotope ratios ($\delta^{13}C$) of CH_4 and dissolved inorganic carbon (DIC), as well as those of the concentrations of EAs were obtained in the hypolimnetic sediments of two additional boreal lake basins showing contrasted O_2 dynamics: one whose hypolimnion remains perennially oxygenated and the other whose hypolimnion becomes anoxic for several months annually. Reaction-transport equations are used to quantify the rates of each OM mineralization pathway and estimate the COS of the substrates fermenting in the sediments. Additional insight into the COS of the fermenting OM in lakes is also provided by applying these equations to similar porewater solute concentration profiles gathered from the scientific literature or from our data repository.

2 Materials and Methods

2.1 Sites and sample collection

This study was carried out in two small, dimictic, oligotrophic and headwater lakes located within 50 km from Québec City, Eastern Canada and having fully forested and uninhabited watersheds (Fig. 1). Lake Tantaré (47°04'N, 71°32'W) is part of the Tantaré Ecological Reserve and has four basins connected by shallow channels and a total surface area of 1.1 km^2. Lake Bédard (47°16'N, 71°07'W), lying in the protected Montmorency Forest, comprises only one small (0.05 km^2) basin. The samples for this study were collected at the deepest sites of Lake Bédard (10 m) and of the westernmost basin of Lake Tantaré (15 m), thereafter referred to as Basin A of Lake Tantaré to remain consistent with our previous studies (e.g., Couture et al., 2008; Clayer et al., 2016). These two sampling sites were selected based on their contrasting O_2 regimes (Fig. 1): Lake Bédard develops an anoxic hypolimnion early in the summer (D'arcy, 1993), whereas the hypolimnion of Lake Tantaré Basin A is perennially oxygenated (Couture et al., 2008). The O_2 diffusion depth in the sediments of Lake Tantaré Basin A, as measured with a microelectrode, does not exceed 4 mm (Couture et al., 2016).

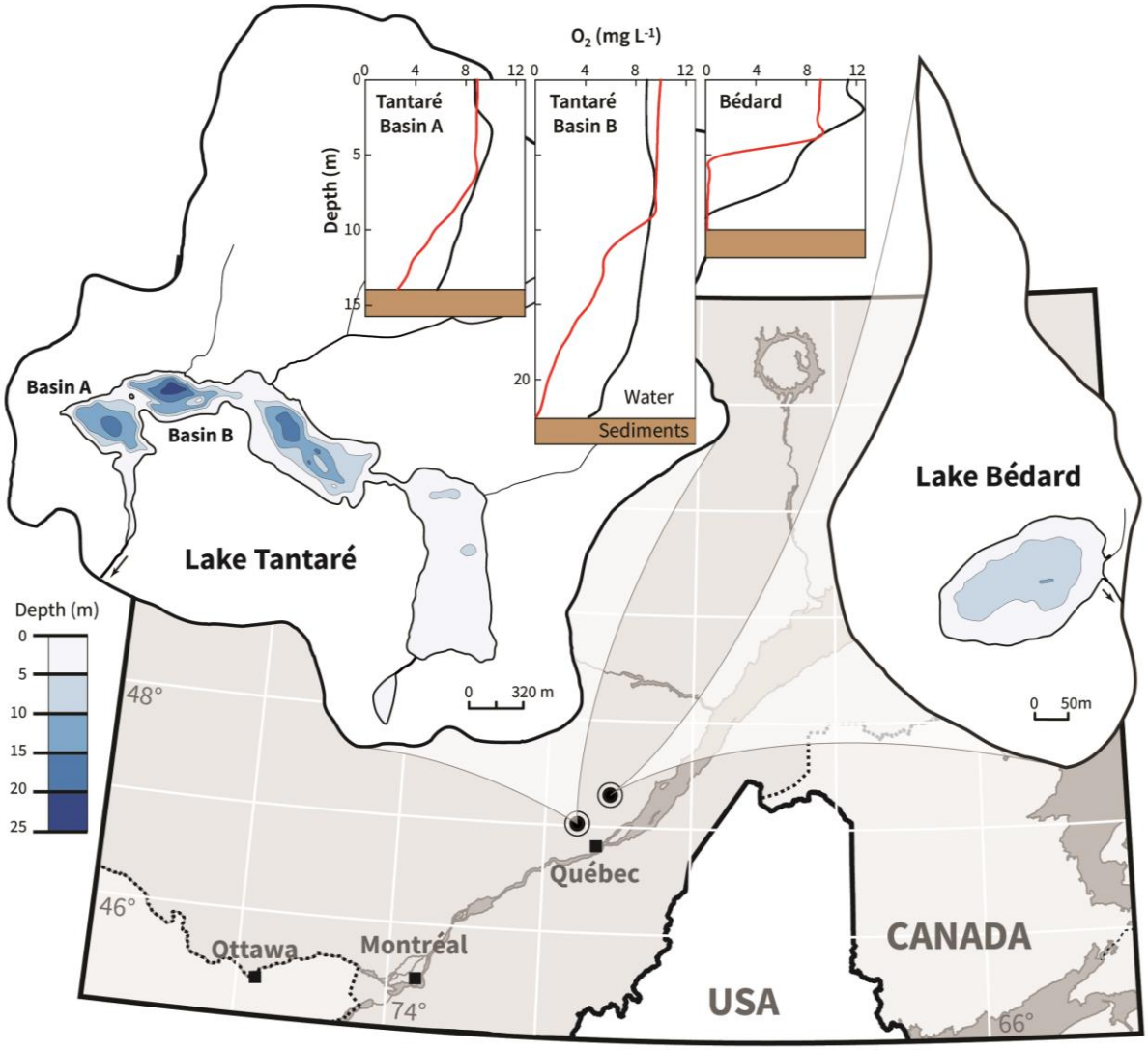

Figure 1: Location map and bathymetry of Lakes Tantaré and Bédard. The bathymetric map of Lake Tantaré was reproduced from the map C-9287 of the Service des eaux de surface of the Québec Ministry of Environment. The map of Lake Bédard was reproduced from D'Arcy (1993). Dioxygen concentrations in the water column of Lake Tantaré basins A and B, and of Lake Bédard are given for June (black lines) and October (red lines).

Sediment porewater samples were acquired by *in situ* dialysis in October 2015 with peepers (Hesslein, 1976; Carignan et al., 1985) deployed by divers within a 25-m² area at the deepest site of each lake basin. Bottom water O_2 concentrations were ~2.5 and < 0.1 mg L^{-1} in Lake Tantaré Basin A and in Lake Bédard, respectively. The acrylic peepers comprised two columns of 4-mL cells, filled with ultrapure water, and covered by a 0.2-µm Gelman HT-200 polysulfone membrane, which allowed porewater sampling from about 23–25 cm below the sediment-water interface (SWI) to 5 cm above this interface (thereafter referred to as overlying water) at a 1-cm depth resolution. Oxygen was removed from the peepers prior to their deployment, as described by Laforte et al. (2005). Four peepers were left in the sediments of

each lake basin for at least 15 d, i.e., a longer time period than that required for solute concentrations in the peeper cells to reach equilibrium with those in the porewater (5–10 d; Hesslein, 1976; Carignan et al., 1985). At least three independent porewater profiles of pH, of the concentrations of CH_4, DIC, acetate, NO_3^-, SO_4^{2-}, Fe and Mn, and of the $\delta^{13}C$ of CH_4 and DIC were generated for the two sampling sites. In Lake Bédard, samples were also collected to determine three porewater profiles of sulfide concentrations (ΣS(−II)). After peeper retrieval, samples (0.9–1.9 mL) for CH_4 and DIC concentrations and $\delta^{13}C$ measurements were collected within 5 minutes from the peeper cells with He-purged polypropylene syringes. They were injected through rubber septa into He-purged 3.85-mL exetainers (Labco Limited), after removal of a volume equivalent to that of the collected porewater. The exetainers were preacidified with 40–80 µL of HCl 1N to reach a final pH ≤ 2. The protocols used to collect and preserve water samples for the other solutes are given by Laforte et al. (2005).

2.2 Analyses

Concentrations and carbon isotopic composition of CH_4 and DIC were measured as described by Clayer et al. (2018). Briefly, the concentrations were analyzed within 24 h of peeper retrieval by gas chromatography with a precision better than 4 % and detection limits (DL) of 2 µM and 10 µM for CH_4 and DIC, respectively. The $^{13}C/^{12}C$ abundance ratios of CH_4 and CO_2 were determined by Mass Spectrometry with a precision of ± 0.2 ‰ when 25 µmol of an equimolar mixture of CH_4 and CO_2 was injected, and results are reported as:

$$\delta^{13}C = 1000\left(\frac{\left(\frac{^{13}C_{solute}}{^{12}C_{solute}}\right)_{sample}}{\left(\frac{^{13}C}{^{12}C}\right)_{standard}} - 1\right) \quad (1)$$

where the subscript solute stands for CH_4 or DIC and the reference standard is Vienna Pee Dee Belemnite (VPDB). Acetate concentration was determined by ion chromatography (DL of 1.4 µM) and those of Fe, Mn, NO_3^-, SO_4^{2-} and ΣS(−II), as given by Laforte et al. (2005).

2.3 Modeling of porewater solutes and the reaction network

The computer program WHAM 6 (Tipping, 2002) was used, as described by Clayer et al. (2016), to calculate the speciation of porewater cations and anions. The solute activities thus

obtained, together with solubility products (K_s), were used to calculate saturation index values (SI = log IAP/K_s, where IAP is the ion activity product).

The following one-dimensional mass-conservation equation (Boudreau, 1997):

$$\frac{\partial}{\partial x}\left(\varphi D_s \frac{\partial [\text{solute}]}{\partial x}\right) + \varphi \alpha_{\text{Irrigation}}([\text{solute}]_{\text{tube}} - [\text{solute}]) + R_{\text{net}}^{\text{solute}} = 0 \quad (2)$$

was used to model the porewater profiles of CH_4, DIC, O_2, Fe and SO_4^{2-}, assuming steady state and negligible solute transport by bioturbation and advection (Clayer et al., 2016). In this equation, $[\text{solute}]$ and $[\text{solute}]_{\text{tube}}$ denote a solute concentration in the porewater and in the animal tubes (assumed to be identical to that in the overlying water), respectively, x is depth (positive downward), φ is porosity, D_s is the solute effective diffusion coefficient in sediments, $\alpha_{\text{Irrigation}}$ is the bioirrigation coefficient, and $R_{\text{net}}^{\text{solute}}$ (in mol cm^{-3} of wet sediment s^{-1}) is the solute net production rate (or consumption rate if $R_{\text{net}}^{\text{solute}}$ is negative). D_s was assumed to be $\varphi^2 D_w$ (Ullman and Aller, 1982), where D_w is the solute tracer diffusion coefficient in water. The values of D_w, corrected for in situ temperature (Clayer et al., 2018), were 9.5 ×10^{-6} cm^2 s^{-1}, 6.01 ×10^{-6} cm^2 s^{-1} and 1.12 ×10^{-5} cm^2 s^{-1} for CH_4, HCO_3^- and CO_2, respectively. The values of $\alpha_{\text{Irrigation}}$ in Lake Tantaré Basin A were calculated as in Clayer et al. (2016), based on an inventory of benthic animals (Hare et al., 1994), and were assumed to be 0 in Lake Bédard since its bottom water was anoxic (Fig. 1).

The $R_{\text{net}}^{\text{solute}}$ values were determined from the average (n = 3 or 4) solute concentration profiles by numerically solving Eq. (2) with the computer code PROFILE (Berg et al., 1998). The boundary conditions were the solute concentrations at the top and at the base of the porewater profiles. In situ porewater O_2 profiles were not measured in Lake Tantaré Basin A. For modeling this solute with PROFILE, we assumed that the $[O_2]$ in the overlying water was identical to that measured in the lake bottom water and equal to 0 below 0.5 cm (based on O_2 penetration depth; Couture et al., 2016). This procedure provides a rough estimate of $R_{\text{net}}^{O_2}$ at the same vertical resolution as for the other solutes. The code PROFILE yields a discontinuous profile of discrete $R_{\text{net}}^{\text{solute}}$ values over depth intervals (zones) which are objectively selected by using the least square criterion and statistical F-testing (Berg et al., 1998). The fluxes of solute transport across the SWI due to diffusion and bioirrigation are also estimated by PROFILE. In

order to estimate the variability in R_{net}^{solute} related to heterogeneity within the 25-m^2 sampling area, additional R_{net}^{solute} values were obtained by modeling the average profiles whose values were increased or decreased by one standard deviation. This variability generally ranges between 2 and 10 fmol cm^{-3} s^{-1}.

The main reactions retained in this study to describe carbon cycling in the sediments of the two lake basins are shown in Table 1. Once oxidants are depleted, fermentation of metabolizable OM (r1) can yield acetate, CO_2 and H_2. The partial degradation of high molecular weight OM (HMW OM) into lower molecular weight OM (LMW OM) can also produce CO_2 (r2, Corbett et al., 2013; Corbett et al., 2015). Acetoclasty (r3) and hydrogenotrophy (r4) yield CH_4. Moreover, CH_4 (r5) and OM (r6) can be oxidized to CO_2 when electron acceptors such as O_2, Fe(III) and SO_4^{2-} are present. Note that the electron acceptors (EAs) NO_3^- and Mn oxyhydroxides can be neglected in these two lake basins (Feyte et al., 2012; Clayer et al., 2016) as well as the precipitation of metal carbonates whose saturation index values are negative ($SI \leq -1.5$) except for siderite (r7) in Lake Bédard (SI = 0.0 to 0.7). Lastly, sulfide oxidation by iron oxides (r8), which can be a source of SO_4^{2-} and H_2 (Holmkvist et al., 2011; Clayer et al., 2018), is also considered.

From Table 1, the net rate of CH_4 production, $R_{net}^{CH_4}$, in the sediments is:

$$R_{net}^{CH_4} = R_3 + R_4 - R_5 \quad (3)$$

where R_3 and R_4 are the rates of acetoclastic (r3) and hydrogenotrophic (r4) production of CH_4, respectively, and R_5 is the rate of DIC production due to CH_4 oxidation (r5). The net rate of DIC production, R_{net}^{DIC}, can be expressed as:

$$R_{net}^{DIC} = R_1 + R_2 + R_3 - R_4 + R_5 + R_6 - R_7 \quad (4)$$

where R_1, R_2 and R_6 are the rates of DIC production due to complete fermentation of labile OM (r1), partial fermentation of HMW OM (r2) and OM oxidation (r6), respectively, and R_7 is the rate of DIC removal by siderite precipitation (r7). It can also be written that:

$$R_{net}^{Ox} = -2R_5 - R_6 \quad (5)$$

where R_{net}^{Ox} is the net reaction rate of all the oxidants (O_2, Fe(III) and SO_4^{2-}) consumption. For simplicity, R_{net}^{Ox} is expressed in equivalent moles of O_2 consumption rate, taking into account

that SO_4^{2-} and Fe(III) have twice and one quarter the oxidizing capacity of O_2, respectively. In practice, the value of R_{net}^{Ox} was calculated by adding those of $R_{net}^{O_2}$, $\frac{1}{4}R_{net}^{Fe(III)}$ and $2R_{net}^{SO_4^{2-}}$ where $R_{net}^{O_2}$, $R_{net}^{Fe(III)}$ and $R_{net}^{SO_4^{2-}}$ were estimated with PROFILE. In this calculation, we assumed that all dissolved Fe is in the form of Fe(II), and that the rate of Fe(II) consumption through reactions r7 is negligible compared to those associated with reactions r5 and r6. Under these conditions, $R_{net}^{Fe(III)} = -R_{net}^{Fe}$.

Table 1: Reactions (r1–r8) considered, their reaction rates (R_1–R_8) and carbon isotopic fractionation factors (α_1–α_7).

Description	Reaction	ID
CO_2 production due to complete fermentation of labile OM [a]		
	$C_xH_yO_z + (x + \nu_1 - z)H_2O \xrightarrow[\alpha_1]{R_1} \left(\frac{x-\nu_1}{2}\right) CH_3COOH + \nu_1 CO_2 + \left(\frac{y}{2} - z + 2\nu_1\right) H_2$	r1
CO_2 production due to partial fermentation of HMW OM [a,b]		
	ν_2 HMW OM $\xrightarrow[\alpha_2]{R_2} \nu_3$ LMW OM $+ \nu_4 CO_2$	r2
Methanogenesis via		
acetoclasty	$CH_3COOH \xrightarrow[\alpha_3]{R_3} CH_4 + CO_2$	r3
hydrogenotrophy	$CO_2 + 4H_2 \xrightarrow[\alpha_4]{R_4} CH_4 + 2H_2O$	r4
CO_2 production due to		
methanotrophy	$CH_4 + 2$ Oxidants $\xrightarrow[\alpha_5]{R_5} CO_2 + 2$ Reducers	r5
OM oxidation	OM + Oxidant $\xrightarrow[\alpha_6]{R_6} CO_2$ + Reducer	r6
Precipitation of siderite	$Fe^{2+} + CO_2 + H_2O \xrightarrow[\alpha_7]{R_7} FeCO_{3(s)} + 2H^+$	r7
H_2 production through a Fe-S cryptic cycle [a,c]		
	$(16 + \nu_5)H_2S + 8FeOOH \xrightarrow{R_8} 8FeS_2 + \nu_5 SO_4^{2-} + (4 + 4\nu_5)H_2 + (16 - 4\nu_5)H_2O + 2\nu_5 H^+$	r8

[a] where ν_1 can have any value between 0 and x, values for ν_2–ν_4 are unknown and ν_5 can have any value between 0 and 1.

[b] HMW OM and LMW OM designate high and lower molecular weight organic matter, respectively.

[c] adapted from Holmkvist et al. (2011)

237 2.4 Modeling of the $\delta^{13}C$ profiles

238 The $\delta^{13}C$ profiles of CH_4 ($\delta^{13}C$-CH_4) and DIC ($\delta^{13}C$-DIC) were simulated with a
239 modified version of Eq. 1 (Clayer et al., 2018):

$$\delta^{13}C = 1000\left(\frac{\left(\frac{[^{13}C]}{[C]}\right)_{sample}}{\left(\frac{^{13}C}{^{12}C}\right)_{standard}} - 1\right) \quad (6)$$

240 where $[C]$ is the total CH_4 or DIC concentration ($[^{12}C]$ can be replaced by [C] since ~99% of C is
241 ^{12}C), and $[^{13}C]$ is the isotopically heavy CH_4 or DIC concentration. Equation 6 allows
242 calculating a $\delta^{13}C$ profile once the depth distributions of $[^{13}C]$ and $[C]$ are known. This
243 information is obtained by solving the mass-conservation equations of C and ^{13}C for CH_4 and
244 DIC. The one-dimensional mass-conservation of [C] is given by Eq. 2 where [solute] is replaced
245 by [C], whereas that for $[^{13}C]$ is the following modified version of Eq. 2 (Clayer et al., 2018):

$$\frac{\partial}{\partial x}\left(\varphi\frac{D_s}{f}\frac{\partial[^{13}C]}{\partial x}\right) + \varphi\alpha_{Irrigation}([^{13}C]_{tube} - [^{13}C]) + \sum_{i=1}^{5}\frac{R_i}{\alpha_i}\left(\frac{\delta^{13}C_i^{reactant}}{1000} + 1\right)\left(\frac{^{13}C}{^{12}C}\right)_{standard} = 0 \quad (7)$$

246 where f, the molecular diffusivity ratio, is the diffusion coefficient of the regular solute divided
247 by that of the isotopically heavy solute, α_i is the isotope fractionation factor in reaction r_i, and
248 $\delta^{13}C_i^{reactant}$ is the $\delta^{13}C$ of the reactant leading to the formation of the solute (CH_4 or DIC) in
249 reaction r_i. Input and boundary conditions used to numerically solve Eqs 2 and 7 for $[C]$ and
250 $[^{13}C]$, respectively, via the bvp5c function of MATLAB® are described in section 3.4 and in
251 section S2 of the Supporting Information (SI).

252 The goodness of fit of the model was assessed with the norm of residuals (N_{res}):

$$N_{res} = \sqrt{\sum_{x=0.5}^{22.5}(\delta^{13}C_m - \delta^{13}C_s)^2} \quad (8)$$

253 where $\delta^{13}C_m$ and $\delta^{13}C_s$ are the measured and simulated $\delta^{13}C$ values, respectively. The norm of
254 residuals (N_{res}) varies between 0 and infinity with smaller numbers indicating better fits.

255 2.5 Data treatment of other data sets

256 To better assess the COS of the fermenting OM in lakes, relevant sets of porewater
257 concentration profiles (CH_4, DIC, EAs, Ca) available from the literature or from our data
258 repository have been modeled with the code PROFILE, as described in section 2.3, to extract
259 their $R_{net}^{CH_4}$, R_{net}^{DIC} and R_{net}^{Ox} profiles. These porewater datasets, described in section S3 of the SI,
260 had been generated by sampling porewater in the hypolimnetic sediments of: i) Lake Bédard and
261 Basin A of Lake Tantaré, at other dates than for this study (Clayer et al, 2016); ii) Basin B of
262 Lake Tantaré (adjacent to Basin A; Fig 1), on four occasions (Clayer et al., 2016; 2018); iii)
263 Williams Bay of Jacks Lake (44°41' N, 78°02' W), located in Ontario, Canada, on the edge of
264 the Canadian Shield (Carignan and Lean 1991); iv) the southern basin of the alpine Lake Lugano
265 (46°00'N, 3°30'E) located in Switzerland, on two occasions (Lazzaretti-Ulmer and Hanselmann
266 1999). All lake basins, except Basin A of Lake Tantaré develop an anoxic hypolimnion.

267 **3 Results**

268 3.1 Solute concentration profiles

269 Differences among the replicate profiles of CH_4, DIC, SO_4^{2-}, ΣS(−II) and Fe (Fig. 2) at
270 the two sampling sites are generally small (except perhaps those of SO_4^{2-} in Lake Bédard) and
271 should be mainly ascribed to spatial variability within the 25-m^2 sampling area. Indeed, the main
272 vertical variations in the profiles are defined by several data points without the sharp
273 discontinuities expected from sampling and handling artifacts. Note that the acetate
274 concentrations, which were consistently low (< 2 µM), are not shown.

275 The low Fe (< 5 µM; Fig. 2f) and CH_4 (< 2 µM; Fig. 2a) concentrations as well as the
276 relatively high SO_4^{2-} concentrations (36 ± 2.1 µM; Fig. 2e) in the sediment overlying water of
277 Lake Tantaré Basin A are all consistent with the [O_2] (~2.5 mg L^{-1}) measured in the bottom
278 water and are indicative of oxic conditions at the sediment surface. The sharp Fe gradients near
279 the SWI indicate an intense recycling of Fe oxyhydroxides (Fig. 2f; Clayer et al., 2016) and the
280 concave-down curvatures in the SO_4^{2-} profiles (Fig. 2e) reveal SO_4^{2-} reduction near the SWI.

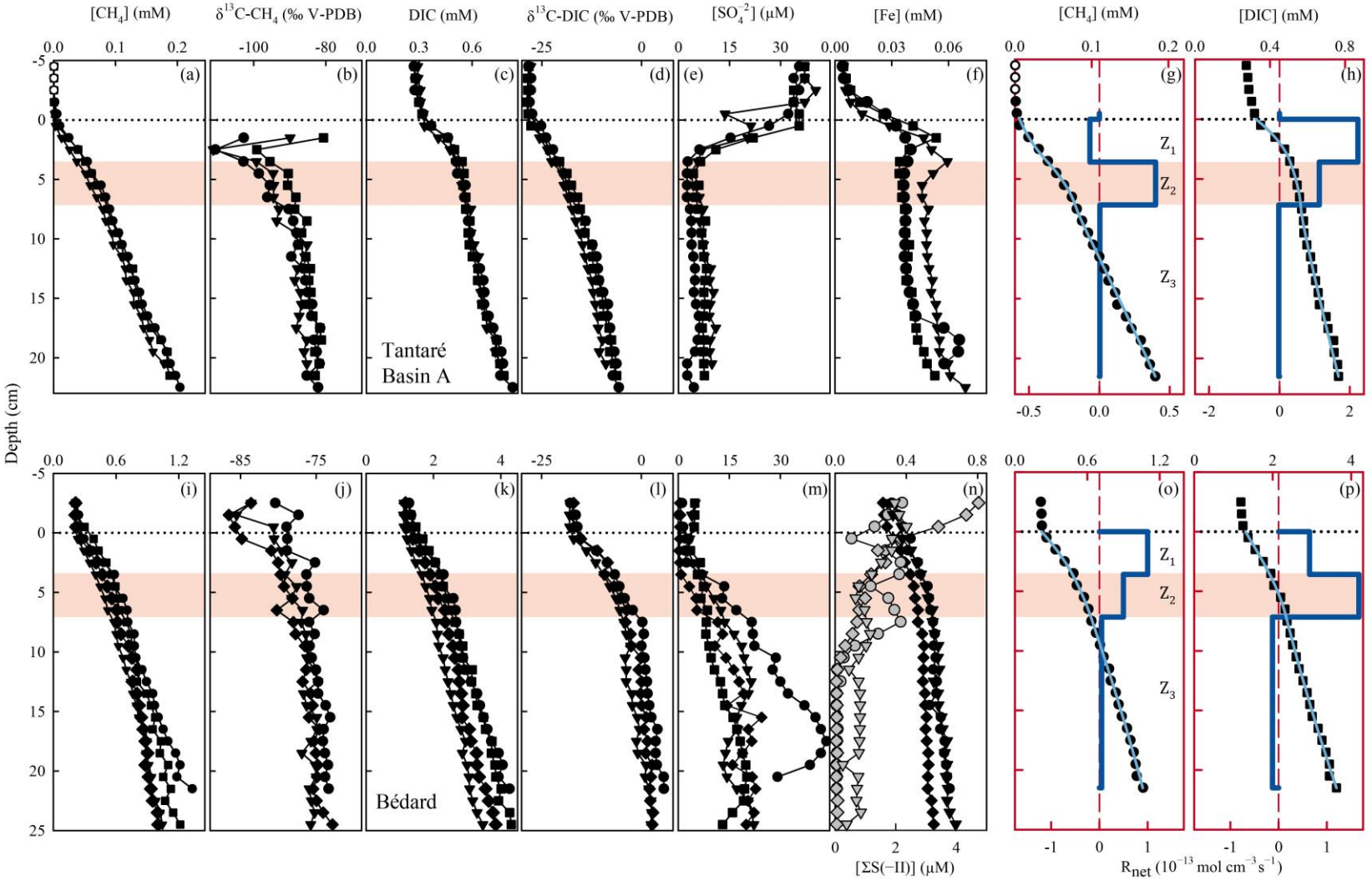

Figure 2 : Replicate porewater profiles of CH4 (a and i), δ13C-CH4 (b and j), DIC (c and k), δ13C-DIC (d and l), SO_4^{2-} (e and m), Fe and ΣS(−II) (f and n), and comparison of the modeled (blue lines) and average (n = 3) measured (symbols) concentration profiles of CH4 (g and o) and DIC (h and p) in Lakes Tantaré Basin A (a–h) and Bédard (i–p). Different symbols indicate data from different peepers and empty symbols are for concentrations below detection limit. The horizontal dotted line indicates the sediment-water interface. The thick and thin blue lines represent the net solute reaction rate (R_{net}^{solute}) and the modeled concentration profiles, respectively. The red area fills correspond to the sediment zones Z2.

In contrast to Lake Tantaré Basin A, high Fe (> 200 µM), measurable CH_4 (> 200 µM) low SO_4^{2-} (2.7 ± 1.4 µM) and detectable ΣS(−II) concentrations in the overlying waters of Lake Bédard (Fig. 2i, m and n) are consistent with anoxic conditions at the sediment surface. The absence of a sharp Fe gradient at the SWI in Lake Bédard suggests that Fe oxyhydroxides were not recycled in these sediments when porewater sampling occurred.

In the two lake basins, SO_4^{2-} concentrations reach a minimum between the SWI and 5 cm depth (Fig. 2e and m), and increase below these depths. Alongside, all Fe profiles show a slight increase downward (Fig. 2f and n) indicating that solid Fe(III) is reduced to produce dissolved Fe. In Lake Bédard, the ΣS(−II) concentrations decrease from the SWI to ~10 cm depth and remain relatively constant below that depth at 0.08 ± 0.06 µM for two of the profiles and at 0.71 ± 0.18 µM for the other one (grey filled triangles in Fig. 2n).

The concentrations of CH_4 (< 1.5 mM; Fig. 2a and i) are well below saturation at 4°C and *in situ* pressure (4.4–5.5 mM; Duan and Mao, 2006), implying that CH_4 ebullition is a negligible CH_4 transport process. The CH_4 values increases from < 2 µM in the overlying water to 0.18–0.20 mM at the base of the Lake Tantaré Basin A profiles (Fig. 2a), and from 0.2–0.5 mM to 1.0–1.4 mM in those of Lake Bédard (Fig. 2i). The three CH_4 profiles from Lake Tantaré Basin A (Fig. 2a) show a modest concave-up curvature in their upper part, close to the SWI, indicative of a net CH_4 consumption, and a convex-up curvature in their lower part, typical of a net CH_4 production. Such trends, however, are not observed in Lake Bédard sediments. The CH_4 profiles from this lake exhibit a convex-up curvature over the whole sediment column, although more pronounced in its upper part (Fig. 2i).

The DIC concentrations consistently increase from 0.27–0.32 mM and 1.2–1.5 mM in the sediment overlying water to 0.76–0.83 mM and 3.5–4.3 mM at the bottom of the profiles in Lake Tantaré Basin A and Lake Bédard, respectively (Fig. 2c and k). All DIC profiles show a similar shape with a slight concave-up curvature in their lower segment and a convex-up curvature in their upper portions.

3.2 Modeled CH_4 and DIC concentration profiles

The modeled [CH_4] and DIC profiles accurately fit the average (n = 3 or 4) data points ($r^2 > 0.996$ and $r^2 > 0.998$ for CH_4 and DIC, respectively; Fig. 2g,h,o and p). The $R_{net}^{CH_4}$ profiles

reveal three zones in each lake basin numbered Z_1, Z_2 and Z_3 from the sediment surface whose boundaries match those defined by the R_{net}^{DIC} profiles. For Lake Tantaré Basin A, Z_1 corresponds to a net CH_4 consumption and Z_2 and Z_3 to net CH_4 production, with the highest rate in Z_2 (Fig. 2g). In contrast, the three zones in Lake Bédard show net CH_4 production with the highest rate in Z_1 and the lowest in Z_3 (Fig. 2o). The R_{net}^{DIC} profiles in both lake basins show a zone of net DIC consumption below two zones of net DIC production with the highest rate values in the Z_1 and Z_2 for Lake Tantaré Basin A and Lake Bédard, respectively.

The $R_{net}^{CH_4}$ and R_{net}^{DIC} profiles displayed in Figure 2 are, among all the possible solutions, the ones that give the simplest rate profile while providing a satisfying explanation of the averaged solute concentration profile as determined by statistical F-testing implemented in the code PROFILE (P value ≤ 0.001 except for the R_{net}^{DIC} profile in Lake Bédard whose P value is ≤ 0.005). As an additional check of the robustness of the depth distribution of $R_{net}^{CH_4}$ and R_{net}^{DIC} provided by PROFILE, we used another inverse model, i.e., Rate Estimation from Concentrations (REC; Lettmann et al., 2012) to model the average CH_4 and DIC profiles. Note that the statistical method, implemented in REC to objectively select the depth distribution of the net reaction rates, i.e., the Tikhonov regularization technique, differs from that of PROFILE. Figure S1 (SI) shows that the two codes predicted mutually consistent $R_{net}^{CH_4}$ and R_{net}^{DIC} profiles, with rate values of similar magnitude. PROFILE was also used in this study to estimate $R_{net}^{SO_4^{2-}}$, R_{net}^{Fe} and R_{net}^{O2} in order to calculate the value of R_{net}^{Ox} in each zone at both sampling sites (see section 2.3 for details). The modeled $[SO_4^{2-}]$ and [Fe] profiles are not shown but, again, they accurately fit the data points ($r^2 > 0.983$). As expected from the contrasting O_2 regimes of the two lake basins, R_{net}^{Ox} values for Lake Tantaré Basin A were one to two orders of magnitude higher than those for Lake Bédard. Note that R_{net}^{O2} was by far the highest contributor to the value of R_{net}^{Ox} in Lake Tantaré Basin A with values of -290 and -72 fmol cm^{-3} s^{-1} in the Z_1 and Z_2, respectively. The values of $R_{net}^{CH_4}$, R_{net}^{DIC} and R_{net}^{Ox} estimated in each zone of each lake basins are reported in Table 2.

Table 2: Net production rates (R_{net}^{solute}) of CH_4, DIC and oxidants obtained with the code PROFILE in the three CH_4 consumption/production zones (Z_1, Z_2 and Z_3) for both sampling sites.

Sampling site ($[O_2]$ in mg L^{-1})	Zones	Depth (cm)	R_{net}^{DIC} (fmol cm^{-3} s^{-1})	$R_{net}^{CH_4}$ (fmol cm^{-3} s^{-1})	R_{net}^{Ox} (fmol cm^{-3} s^{-1})
Tantaré Basin A (2.5)	Z_1	0–3.6	223	−7	−335
	Z_2	3.6–7.2	113	39	−103
	Z_3	7.2–21.5	−2	1	
Bédard (<0.1)	Z_1	0–3.6	65	100	−6.5
	Z_2	3.6–7.2	167	50	−4.5
	Z_3	7.2–21.5	−13	5	

3.3 The $\delta^{13}C$ profiles

The $\delta^{13}C$-DIC values increase from −28.2 ± 0.4 ‰ and −17.2 ± 0.7 ‰ in the overlying water to −5.1 ± 1.0 ‰ and 3.6 ± 1.7 ‰ at the base of the profiles in Lake Tantaré Basin A and Lake Bédard, respectively (Fig. 2d and l). Similarly, the $\delta^{13}C$-CH_4 values in Lake Bédard increase steadily from −82.5 ± 3.3 ‰ in the overlying water to −74.0 ± 1.5 ‰ at 24.5 cm depth (Fig. 2j). Regarding Lake Tantaré Basin A, the CH_4 concentrations above 1.5 cm depth were too low for their $^{13}C/^{12}C$ ratio to be determined. Starting at 1.5 cm depth, the $\delta^{13}C$-CH_4 values first decrease from −91.1 ± 11.1 ‰ to −107.0 ± 6.8 ‰ at 2.5 cm depth and then increase progressively to −83.5 ± 1.6 ‰ at the base of the profiles (Fig. 2b). Note that a shift toward more positive $\delta^{13}C$-CH_4 values upward, generally attributed to the oxidation of CH_4 (Chanton et al., 1997; Norði et al., 2013), is only observed in the profiles of Lake Tantaré Basin A (Fig. 2b).

As shown in Fig. S2 (SI), the isotopic signatures of nearly all samples from the two lake basins fall within the ranges reported for hydrogenotrophic methanogenesis, i.e., CO_2 reduction, in a $\delta^{13}C$-CO_2 *vs* $\delta^{13}C$-CH_4 graph similar to that proposed by Whiticar (1999). Indeed, the values of $\delta^{13}C$-CH_4 which are lower than -70 ‰ over the whole profiles in the two lake basins, and the large difference (67 to 92 ‰) between the $\delta^{13}C$ of gaseous CO_2 ($\delta^{13}C$-CO_2) and $\delta^{13}C$-CH_4, strongly contrast with the typical $\delta^{13}C$-CH_4 values (−68 to −50 ‰) and with the difference between $\delta^{13}C$-CO_2 and $\delta^{13}C$-CH_4 (39 to 58 ‰) reported for acetoclasty (Whiticar, 1999). The $\delta^{13}C$ results reported previously for another basin of Lake Tantaré (Basin B; Clayer et al., 2018) show also in the hydrogenotrophy domain in Fig. S2.

3.4 Modeled $\delta^{13}C$ profiles

In order to model the $\delta^{13}C$ profiles with Eq. 6, accurate profiles of $[C]$ and $[^{13}C]$ need first to be determined by numerically solving Eqs. 2 and 7, respectively. The modeled profiles of $[CH_4]$ and DIC obtained with Eq. 2 replicated well the measured profiles of these two solutes when the depth distributions of $R_{net}^{CH_4}$ or R_{net}^{DIC} provided by PROFILE (Table 2) and those of D_s, $\alpha_{Irrigation}$ and φ were used as inputs in Eq. 2, and when measured CH_4 or DIC concentrations at the top and bottom of the profiles were imposed as boundary conditions. Getting a truthful profile of $[^{13}C]$ with Eq. 7 requires, however, accurate values of $\delta^{13}C_i^{reactant}$, α_i, and R_i for each of the reactions given in Table 1, and of f for both CH_4 (f-CH_4) and DIC (f-DIC). The multi-step procedure followed to obtain the best $[^{13}C]$ profiles for CH_4 and DIC is described in section S2 (SI). This modeling exercise revealed that $R_3 = 0$ for all the zones in the sediments of both lake basins, thus confirming that practically all CH_4 is produced through hydrogenotrophy, as inferred above from the $\delta^{13}C$ values.

The best fits between the simulated and measured $\delta^{13}C$ profiles of CH_4 and DIC for Lake Tantaré Basin A and Lake Bédard (red lines in Fig. 3) were obtained with the f, α_i and R_i values displayed in Table 3. The optimal α_i and f values were within the ranges reported in the literature for both lake basins, except for the lower-than-expected value of α_2 (0.984) in the Z_2 of Lake Bédard. Note that α_3 is not given in Table 3 since the modeling of the $\delta^{13}C$ profiles of CH_4 and DIC indicates that $R_3 = 0$ (see section S2.2.2.1 in the SI). Optimal values for α_4, α_5 and f-CH_4 for both lake basins were also similar to those reported in our previous study on Lake Tantaré Basin B (Clayer et al., 2018).

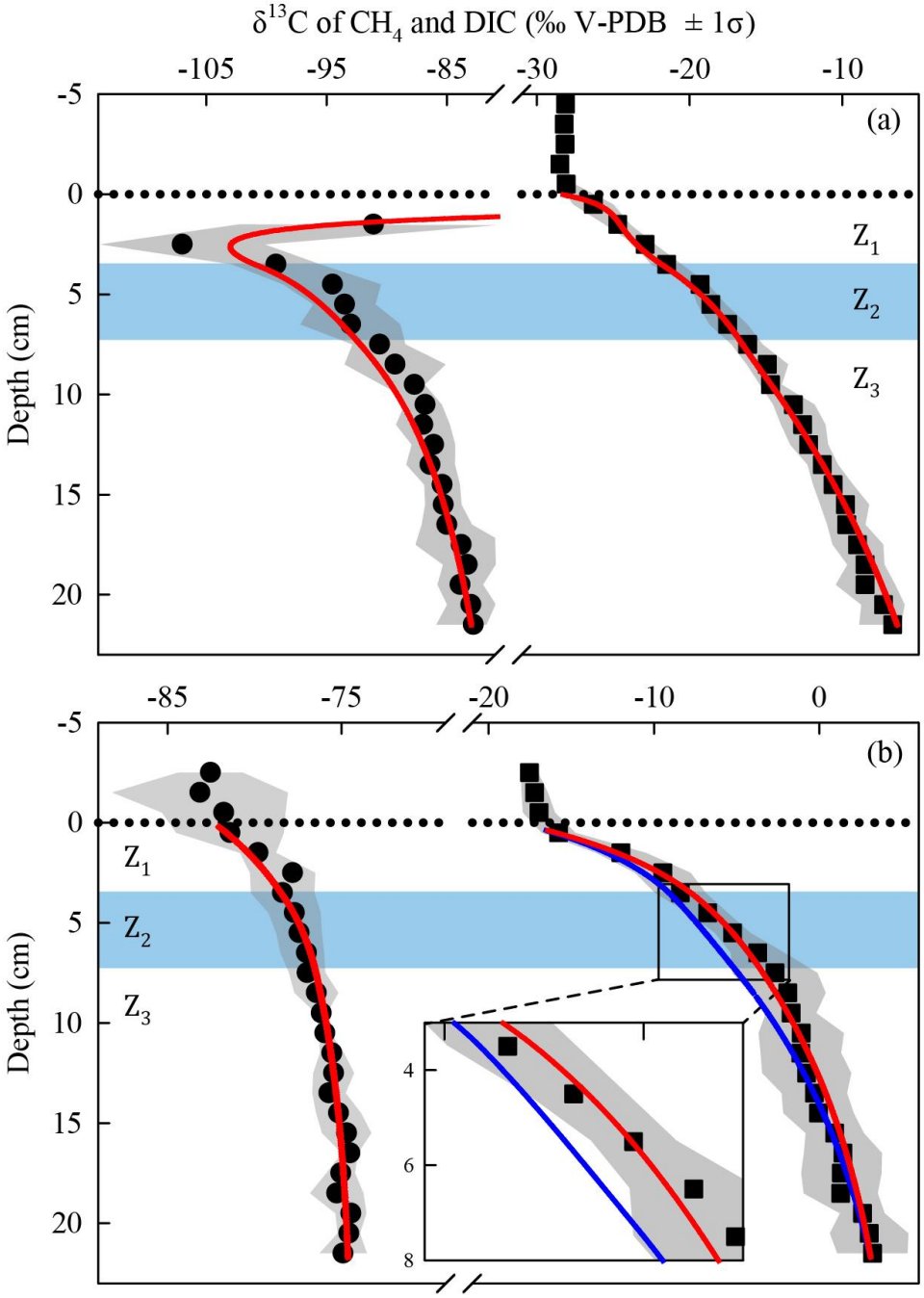

Figure 3 : Comparison of the simulated (lines) and measured average (n = 3) $\delta^{13}C$ profiles of CH_4 (circles) and DIC (squares) in the porewater of Lake Tantaré Basin A (a) and Lake Bédard (b). The horizontal dotted line indicates the sediment-water interface. The variability in $\delta^{13}C$ values (± one standard deviation – σ) related to the spatial heterogeneity within the sampling area is shown by the grey area fills. The zone Z_2 is delimited by the blue area fill. In panel b, the blue lines are the profiles simulated with the default rate values and optimal α_i and f values as described in section S2.2.1. The red lines in panel (b) are the profiles simulated with α_2 values of 0.980–0.984 (see section 4.1 for details).

Table 3: Molecular diffusivity ratio of CH_4 (f-CH_4) as well as the isotopic fractionation factors (α_1, α_2, α_4–α_7) and rates (R_1, R_2, R_4–R_7; fmol cm^{-3} s^{-1}) of each reaction involved in OM mineralization in each zone and for the whole sediment column (ΣR_i ; fmol cm^{-2} s^{-1}) corresponding to the lowest values of N_{res}. At both study sites, R_3 was shown to be negligible. See section S2 of the SI for details.

Study site	Zones	f-CH_4	α_1	α_2	α_4	α_5	α_6	α_7	R_1	R_2	R_4	R_5	R_6	R_7
Tantaré Basin A	Z_1	1.003	1.000	-	1.094	1.024	1.000	-	132	-	119	126	84	-
	Z_2	1.003	1.000	-	1.087	1.005	1.000	-	126	-	78	39	26	-
	Z_3	1.003	-	-	1.085	-	-	-	-	-	1	-	-	-
	ΣR_i								931	-	721	592	394	-
Bédard	Z_1	1.003	1.000	-	1.074	-	-	-	165	-	100	-	-	-
	Z_2	1.003	-	0.984[a]	1.074	-	-	-	72[b]	145[b]	50	-	-	-
	Z_3	1.003	-	-	1.074	-	-	0.995	-	-	5	-	-	8
	ΣR_i								853	522	612	-	-	114

[a]the optimal value of α_2, given here is for a COS value of −1.5, varies slightly with the COS value (see section S2.2.2.3 of the SI).

[b]the value of R_1 and R_2, given here is for a COS value of −1.5, varies with the COS value (see section S2.2.2.3 of the SI).

4 Discussion

4.1 Organic matter mineralization pathways at the sampling sites

The porewater data as well as the combined modeling of carbon isotopes and concentration profiles, allows to highlight key OM mineralization mechanisms and to quantify the relative contribution of methanogenesis and fermentation to OM degradation at both sampling sites The ^{13}C isotopic signatures, i.e., highly negative values of $\delta^{13}C$-CH_4 and large differences between $\delta^{13}C$-CO_2 and $\delta^{13}C$-CH_4 (section 3.3 and Fig. S2 in the SI), as well as the modeling of the $\delta^{13}C$-CO_2 and $\delta^{13}C$-CH_4 profiles (section S2.2.2.1 and Fig S4a and b in the SI) all point to hydrogenotrophy as being the only pathway for methanogenesis in the two lake basins. The dominance of hydrogenotrophy is consistent also with the finding that acetate concentrations were close to or below DL in the porewater samples. Under the condition that acetocalsty is negligible (i.e., $x = \nu_1$), reaction r1 from Table 1 becomes:

$$C_xH_yO_z + (2x - z)H_2O \xrightarrow{R_1} xCO_2 + (2x + \frac{y}{2} - z)H_2 \qquad (9)$$

Methanogenesis was also reported to be essentially hydrogenotrophic in the sediments of Basin B of Lake Tantaré (Clayer et al 2018). The absence of acetoclasty in the sediments of the oligotrophic lakes Bédard and Tantaré is consistent with the consensus that hydrogenotrophy becomes an increasingly important CH_4 production pathway: i) when labile OM is depleted

(Whiticar et al., 1986; Chasar et al., 2000; Hornibrook et al., 2000), ii) with increasing sediment/soil depth (Hornibrook et al., 1997; Conrad et al., 2009), or iii) with decreasing rates of primary production in aquatic environments (Wand et al., 2006; Galand et al., 2010).

The modelling of concentrations and $\delta^{13}C$ profiles revealed that oxidative processes occurred essentially in the upper 7 cm of the sediments of the perennially oxygenated Lake Tantaré Basin A, i.e., mainly in the Z_1 and, to a lesser extent, in the Z_2 (Table 3 and sections S2.1.2.1 and S2.1.2.2 of the SI). Moreover, it showed that methanotrophy was the dominant oxidative reaction in these sediment layers since 75% of the oxidants were consumed through r5 (section S2.2.2.2 of the SI). This outcome is consistent with several studies showing that methanotrophy occurs at higher rates than OM oxidation at low EA concentrations (Sivan et al., 2007; Pohlman et al., 2013; Kankaala et al., 2013; Thottahil et al., 2019). Methanotrophy is also evidenced in the Z_1 of this lake basin by the negative $R_{net}^{CH_4}$ value and by a shift of the $\delta^{13}C\text{-}CH_4$ profiles to more positive values in their upper part (Fig. 2b and g). Use of Eq. 2 to model the EAs profiles with the code PROFILE predicts that O_2 was by far the main EA involved either directly, or indirectly via the coupling with the Fe or S cycles, in the oxidative processes. Indeed, comparing the values of R_{net}^{O2} and R_{net}^{Ox} (see Section 3.2 and Table 2) shows that O_2 accounts for 87% and 70% of the oxidants consumed in the Z_1 and Z_2 of Lake Tantaré Basin A, respectively. Since O_2 penetration in the sediment by molecular diffusion is limited to ~4-mm, a significant amount of O_2 is predicted by Eq. 2 to be transported deeper in the sediment through bioirrigation. The predominance of O_2 among the EAs consumed in the sediments is consistent with our previous study in this basin of Lake Tantaré (Clayer et al., 2016). Given that methanotrophy is the dominant oxidative process and that O_2 is the main oxidant consumed, it is probable that aerobic oxidation of methane prevails over its anaerobic counterpart in this lake basin. This is in line with the common thinking that CH_4 oxidation in freshwater lake sediments is carried out by methanotrophs essentially in the uppermost oxic sediment layer (Bastviken et al., 2008 and references therein).

The sharp upward depletion in $^{13}C\text{-}CH_4$ leading to a minimum $\delta^{13}C\text{-}CH_4$ value at 2.5 cm depth in Lake Tantaré Basin A sediments (Fig. 3a) was unanticipated since, according to the modeling with the code PROFILE, it occurs in the methanotrophic zone, i.e., where the remaining CH_4 is expected to be ^{13}C-enriched as a result of CH_4 oxidation. Marked $^{13}C\text{-}CH_4$

444 depletions at the base of the sulfate-methane transition zone, where CH_4 is consumed via SO_4^{2-}
445 reduction, have often been observed in marine sediments (Burdige et al., 2016 and references
446 therein). Such features are generally attributed to the production of CH_4 by hydrogenotrophy
447 from the ^{13}C-depleted DIC resulting from the anaerobic CH_4 oxidation, a process referred to as
448 intertwined methanotrophy and hydrogenotrophy (e.g., Borowski et al., 1997; Pohlman et al.,
449 2008; Burdige et al., 2016). Here the modelled $\delta^{13}C$-CH_4 profile captured the minimum in $\delta^{13}C$-
450 CH_4 in the Z_1 by simply assuming concomitant hydrogenotrophy and methanotrophy in this zone
451 and an upward-increasing α_4 value from 1.085 in the Z_3 to 1.094 in the Z_1 (section S2.2.1 of the
452 SI). These α_4 values remain within the range reported for this isotope fractionation factor (Table
453 S1 in the SI). A small variation with sediment depth in the fractionation factor α_4 is arguably
454 possible since its value depends on the types of microorganisms producing CH_4 (Conrad 2005).
455 The possibility that a depth variation in this isotope fractionation factor could explain some of
456 the minima in $\delta^{13}C$-CH_4 reported in other studies should be considered.

457 In the Z_2 of Lake Bédard, the net rate of DIC production (i.e., 167 fmol cm^{-3} s^{-1}) was
458 more than 3 times that of CH_4 production (50 fmol cm^{-3} s^{-1}; Table 2). Given that the R_{net}^{Ox} was
459 negligible in this zone (i.e., $R_5 = R_6 = 0$), we obtain from Eqs 3 and 4 and Table 2 that $R_{net}^{CH_4} =$
460 $R_4 = 50$ fmol cm^{-3} s^{-1} and $R_{net}^{DIC} = R_1 + R_2 - R_4 = 167$ fmol $cm^{-3}s^{-1}$ (see section S2.1.2.2
461 of the SI). Should we assume that DIC production by r2 is negligible, i.e., $R_2 = 0$, a R_1/R_4 ratio of
462 4.3 would be obtained. This high ratio indicates that DIC was not produced by hydrogenotrophy
463 (r4) coupled to fermentation (r1) alone in the Z_2 of this lake. Indeed, methanogenesis through the
464 coupling of these two reactions yields a R_1/R_4 ratio of 2 if the fermenting substrate is
465 carbohydrates (COS of 0) and lower than 2 if the fermenting substrate has a negative COS value.
466 We thus attributed the production of the additional DIC to the partial fermentation of HMW OM,
467 an assumed non-fractionating process reported to occur in wetlands (Corbett et al., 2015). The
468 better fitting of the $\delta^{13}C$-DIC profile when α_2 is set to 0.980–0.984 rather than to 1.000 in the Z_2
469 (compare the blue and red lines in Fig. 4b) suggests that C fractionates during this partial
470 fermentation process.

471 Table 3 displays the depth-integrated reaction rates (ΣR_i) over the top 21cm of the
472 sediment column which are given by:

$$\Sigma R_i = \sum_{j=1}^{3} \Delta x_j R_i \quad (10)$$

where Δx_j (cm) is the thickness of the zone Z_j. In this calculation, we assume that other zones of CH_4 or DIC production are absent below 21 cm. Values of ΣR_i clearly show that anaerobic carbon mineralization reactions (fermentation and methanogenesis) are important contributors to the overall OM mineralization in the two studied lake basins. Indeed, the sum of the rates of CH_4 production (ΣR_4), DIC production due to CH_4 formation ($\Sigma R_1 - \Sigma R_4$) and HMW OM partial fermentation (ΣR_2) represents 49% and 100% of the total OM degradation rate ($\Sigma R_1 + \Sigma R_2 + \Sigma R_5 + \Sigma R_6$) in the sediment of lakes Tantaré Basin A and Bédard, respectively. The contribution of anaerobic mineralization for Lake Tantaré Basin A is about 1.6 times higher than the average of 30% reported for this lake basin in a previous study (Clayer et al., 2016). This significant discrepancy arises because these authors, in the absence of isotopic data to adequately constrain the R_i values, assumed that $R_4 = 0$ in the net methanotrophic zone Z_1. Should we make the same assumption in the present study, we would also estimate that fermentation and methanogenesis represent only 30% of the total rate of OM degradation in the oxygenated Lake Tantaré Basin A and we would thus underestimate the importance of methanogenesis. The inclusion of $\delta^{13}C$ data in the present modeling study thus allowed to better constrain the effective rates of CH_4 production (R_4).

4.2 Organic substrates for methanogenesis at the sampling sites

Table 3 indicates that hydrogenotrophy (r4) coupled to the complete fermentation of OM (r1) produces CH_4 at higher rates (R_4) than DIC ($R_1 - R_4$) in the Z_1 and Z_2 of both lake basins. This outcome is inconsistent with the equimolar production of CH_4 and DIC expected from the fermentation of glucose ($C_6H_{12}O_6$), the model molecule used to represent labile OM in diagenetic models (Paraska et al., 2014), thus suggesting that the fermentation of this compound is not the exclusive source of the H_2 required for hydrogenotrophy. Had OM been represented by $C_6H_{12}O_6$ in r1, the rate of H_2 production by this reaction would have been twice that of CO_2, i.e., $2R_1$. For its part, the rate of H_2 consumption through hydrogenotrophy is four times that of the CH_4 production, i.e., $4R_4$. Hence, an additional H_2 production at rates of up to 212 and 70 fmol cm^{-3} s^{-1}, i.e., $4R_4 - 2R_1$, is needed to balance the H_2 production rate expected from the fermentation

of $C_6H_{12}O_6$ and the H_2 consumption rate by hydrogenotrophy observed in the sediments of Lake Tantaré Basin A and Lake Bédard, respectively. As discussed by Clayer et al. (2018), this additional production rate of H_2 could be provided by a cryptic Fe-S cycle such as r8 (Table1), or by the production of CH_4 via the fermentation of organic substrates more reduced than glucose.

The progressive downward increases in dissolved Fe and SO_4^{2-} (Fig. 2e, f, m and n) below ~5 cm depth and decrease in ΣS(−II) (Fig. 2n) observed in the porewaters support a production of H_2 from r8 in both lakes. However, modeling the appropriate solute profiles with the code PROFILE indicates that the production rates of dissolved Fe (<10 fmol cm^{-3} s^{-1}) and SO_4^{2-} (<1 fmol cm^{-3} s^{-1}) and the consumption rate of ΣS(−II) (<1 fmol cm^{-3} s^{-1}) are about one order of magnitude too low to explain the missing H_2 production rate in both basins. Moreover, in the Z_1 and Z_2 of Lake Tantaré Basin A, the rate of solid Fe(III) reduction (<3 fmol cm^{-3} s^{-1}; calculated from Liu et al. 2015) is much lower than that required from r8 (i.e., 1 to 2 times the additional H_2 production of $4R_4 - 2R_1$; 70–424 fmol cm^{-3} s^{-1}) to produce sufficient amounts of H_2 to sustain the additional hydrogenotrophy. Given these results, we submit that a cryptic Fe-S cycle, if present, would contribute only minimally to the missing rate of H_2 production, and that the fermentation of reduced organic compounds could provide a better explanation to the imbalance between the H_2 production and consumption rates.

Since CH_4 is produced by hydrogenotrophy in the two lake basins ($\chi_H = 1$), Eqn. S15 (section S2.2.2. of the SI) describing the COS of the fermenting organic substrate $C_xH_yO_z$ simplifies as:

$$\mathrm{COS} = -4\left(\frac{2\left(\mathrm{R}_{\mathrm{net}}^{\mathrm{CH_4}} - \frac{1}{2}\chi_{\mathrm{M}}\mathrm{R}_{\mathrm{net}}^{\mathrm{Ox}}\right) - \mathrm{R}_1}{\mathrm{R}_1}\right) \qquad (11)$$

where χ_M is the fraction of oxidants consumed through methanotrophy. Combining Eqs. S7 and S5 of the SI with Eq. 11, we obtain:

$$\mathrm{COS} = -4\left(\frac{\mathrm{R}_{\mathrm{net}}^{\mathrm{CH_4}} - \mathrm{R}_{\mathrm{net}}^{\mathrm{DIC}} - \mathrm{R}_{\mathrm{net}}^{\mathrm{Ox}} + \mathrm{R}_2}{\mathrm{R}_{\mathrm{net}}^{\mathrm{DIC}} + \mathrm{R}_{\mathrm{net}}^{\mathrm{CH_4}} + (1-\chi_{\mathrm{M}})\mathrm{R}_{\mathrm{net}}^{\mathrm{Ox}} - \mathrm{R}_2}\right) \qquad (12)$$

Introducing the values of $\mathrm{R}_{\mathrm{net}}^{\mathrm{CH_4}}$, $\mathrm{R}_{\mathrm{net}}^{\mathrm{DIC}}$, $\mathrm{R}_{\mathrm{net}}^{\mathrm{Ox}}$ and R_2 (Table 2 and 3) into Eq. 12, we calculate COS values of −3.2 and −0.9 for the Z_1 and Z_2 of Lake Tantaré Basin A, respectively,

and of −1.0 to −1.1 for the Z_1 of Lake Bédard, respectively. Note that we were unable to constrain with Eq. 12 the COS for the Z_2 of Lake Bédard since we had to assume a COS value to estimate R_2 and the COS has no influence of the modelled $\delta^{13}C$ profiles (section S2.2.2.3 of the SI). Negative COS values between −0.9 and −1.1 suggest that fermenting OM in the sediments of the two lake basins would be better represented by a mixture of fatty acids and fatty alcohols than by carbohydrates, as suggested by Clayer et al. (2018) for the sporadically anoxic Lake Tantaré Basin B. For its part, the highly negative COS value of −3.2 calculated for the Z_1 of Lake Tantaré Basin A is unreasonable, and the inaccuracy of the COS determination in this lake basin is discussed in section 4.3.

4.3 Reduced organic compounds as methanogenic substrates in lake sediments

In order to better appraise the COS of the fermenting OM in lakes, relevant datasets of porewater solute concentration profiles were gathered from our data repository and from a thorough literature search. To be able to obtain by reactive-transport modeling the R_{net}^{solute} required to calculate the COS with Eq. 12, the datasets had to: (i) comprise porewater concentration profiles of CH_4 and DIC and, ideally, those of the EAs; (ii) reveal a net methanogenesis zone, and iii) enable the carbonate precipitation/dissolution contribution to the DIC concentrations to be estimated. Detailed information on the origin and processing of the 17 selected datasets, acquired in 6 different lake basins from one sub-alpine and three boreal lakes sampled at various dates and/or depths, is given in section S3 of the SI. The CH_4 and DIC porewater profiles determined at hypolimnetic sites of these lake basins and their modeling with the code PROFILE are shown in Fig. 4, whereas the $R_{net}^{CH_4}$, R_{net}^{DIC} and R_{net}^{Ox} values determined from this modeling are regrouped in Table 4. The COS values displayed in Table 4 for all lake basins and dates were calculated by substituting the appropriate $R_{net}^{CH_4}$, R_{net}^{DIC} and R_{net}^{Ox} values in Eq. 12 and assuming that $R_2 = 0$. This latter assumption was not required Lake Tantaré Basin A (October 2015) and Lake Bédard (October 2015) for which R_2 values were known (Table 4). Equation 12 indicates that any DIC contribution from r2 would yield lower COS values than those reported in Table 4. The value of χ_M was assumed to be alternately 0 and 1 to provide a range of COS values. The only exception was Lake Tantaré Basin A in October 2015 for which χ_M is known to be 0.75 (section S2.2.2.2 of the SI). Note that although Eq. 12 was derived with

the assumption that methanogenesis was hydrogenotrophic ($\chi_H = 1$), assuming that CH_4 was produced by acetoclasty ($\chi_H = 0$) would yield the same expression.

Table 4: Net reaction rates (R_{net}^{solute}; fmol cm^{-3} s^{-1}) of CH_4, DIC and oxidants in the zone with the highest production rate of CH_4 as well as the O_2 concentration in the bottom water ([O_2] in mg L^{-1}), the R_2 rates (fmol cm^{-3} s^{-1}) and the average carbon oxidation state (COS) of the fermenting OM at the origin of CH_4 calculated with Eq. (12) at both study sites, Lake Tantaré Basin B (Fig. 1), Jacks Lake (Carignan and Lean 1991) and Lake Lugano (Lazzaretti-Ulmer & Hanselmann 1999) for various sampling dates.

Lake Basin	Sampling date	[O_2]	R_{net}^{DIC}	$R_{net}^{CH_4}$	R_{net}^{Ox}	R_2	Reference	COS[a]	
								Min.	Max.
Tantaré Basin A, 15 m	Oct 2015 – Z_1	3.5	223	−7	−335	0	this study	−3.2	−3.2
	Oct 2015 – Z_2	3.5	113	39	−103	0	this study	−0.9	−0.9
	Jul 2012	6.0	143	245	−66	-	1	−2.1	−1.7
	Sep 2006	4.0	89	33	−45	-	1	0.4	0.6
	Oct 2005	3.1	202	48	−44	-	1	1.8	2.1
	Sep 2004	4.6	99	45	−60	-	1	−0.3	−0.2
Tantaré Basin B, 22 m	Oct 2014	< 0.1	42	116	−1	-	2	−1.9	−1.9
	Oct 2011	0.4	279	783	−12	-	1	−2.0	−1.9
	Jul 2007	4.1	283	1147	−20	-	1	−2.5	−2.5
	Oct 2006	< 0.1	442	825	−2	-	1	−1.2	−1.2
Bédard, 10 m	Oct 2015 – Z_1	< 0.1	65	100	−6.5	0	this study	−1.1	−1.0
	Oct 2003	< 0.1	205	408	−13	-	3	−1.4	−1.4
Jacks Lake, 15 m	Sep 1981	na	284	514	-	-	4	−1.2	−1.2
Jacks Lake, 22 m	Sep 1981	na	904	2030	-	-	4	−1.5	−1.5
Lugano, Melide, 85 m	Mar 1989	2.0	228	388	−83	-	5	−1.8	−1.6
Lugano, Melide, 85 m	Jun 1989	< 0.1	45	97	−1	-	5	−1.5	−1.5
Lugano, Figino, 95 m	Mar 1989	4.0	1168	1903	−234	-	5	−1.4	−1.3
Lugano, Figino, 95 m	Jun 1989	< 0.1	237	355	−19	-	5	−1.0	−0.9

[a] Minimum and Maximum COS values were obtained by setting χ_M to 0 and 1 in Eq. (12), except for Tantaré Basin A in October 2015 for which χ_M is known to be 0.75.

References: (1) Clayer et al. (2016), (2) Clayer et al. (2018), (3) see Supporting Information, (4) Carignan and Lean (1991), (5) Lazzaretti-Ulmer & Hanselmann (1999).

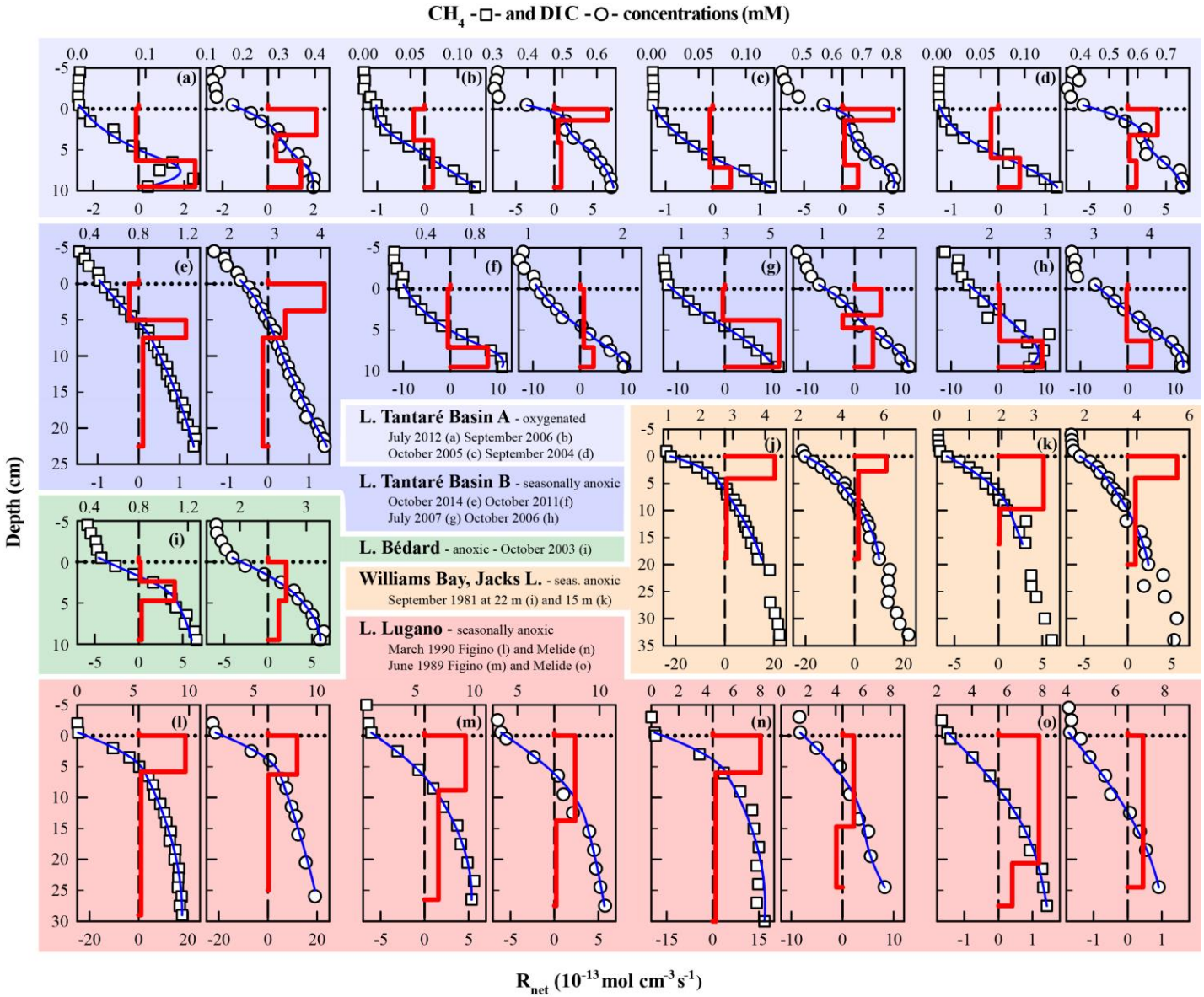

Figure 4 : Comparison of the modeled (blue lines) and average (n = 3) measured concentration profiles of CH4 (squares) and DIC (circles) in Lakes Tantaré Basin A (a–d) and Basin B (a–h), Bédard (i), Jacks Lake (j–k) and Lake Lugano (l–o) at various sampling dates. The thick red lines represent the net solute reaction rate (R_{net}^{solute}).

566 According to Table 4 the COS values are systematically negative at all dates for Lake
567 Tantaré Basin B, Lake Bédard, Jacks Lake and the two sites of Lake Lugano, and they vary
568 generally between −0.9 and −1.9, with the exception of a value of −2.5 obtained for Lake
569 Tantaré Basin B in July 2007. This latter value is likely too low to be representative of
570 fermenting material and should be rejected. The mean (± SD) COS values are −1.7 ± 0.4 for
571 Lake Tantaré Basin B, −1.4 ± 0.4 for Lake Bédard, −1.4 ± 0.2 for Jacks Lake and −1.4 ± 0.3 for
572 Lake Lugano. These COS values, representative of a mixture of fatty acids (COS of −1.0 for C4-
573 fatty acids to about −1.87 for C32-fatty acids) and of fatty alcohols (COS = −2.00), strongly
574 supports the idea that methanogenesis in boreal lakes sediments, as well as in the sediments of
575 other types of lakes, is fueled by more reduced organic compounds than glucose. Lipids such as
576 fatty acids and fatty alcohols with similar COS are naturally abundant in sediments to sustain the
577 estimated rates of CH_4 and DIC production during fermentation (Hedges and Oades, 1997;
578 Cranwell, 1981; Matsumoto, 1989; Burdige, 2006). As discussed by Clayer et al. (2018) the most
579 labile organic compounds (i.e., proteins and carbohydrates) can be rapidly degraded during their
580 transport through the water column and in the uppermost sediment layer, leaving mainly lipids as
581 metabolizable substrates at depths where fermentation and methanogenesis occurs. This
582 interpretation is consistent with thermodynamic and kinetic evidences that proteins and
583 carbohydrates are more labile and are degraded faster than lipids (LaRowe and Van Cappellen,
584 2011).

585 The COS values determined for the perennially oxygenated Basin A of Lake Tantaré
586 (mean of −0.6 ±1.1; range of −3.2 to 2.1; Table 4) are much more variable than for the five other
587 lake basins which undergo seasonal anoxia. Moreover, the COS values estimated for October
588 2015 in the Z_1 (−3.2), September 2016 (0.4–0.6) and October 2005 (1.8–2.1) are unrealistic.
589 Indeed, the very negative value of −3.2 does not correspond to any degradable compound under
590 anoxic conditions, whereas the positive values of 0.4–0.6 and 1.8–2.1 would involve either
591 amino acids and nucleotides which are very labile (Larowe and Van Cappellen 2011) and tend to
592 be degraded in the water column (Burdige 2007) or oxidized compounds, such as ketones,
593 aldehydes and esters, known to be quickly reduced to alcohols. These observations indicate that
594 the COS determination in this lake basin is unreliable. The misestimation of the COS can
595 probably not be explained by the presence of O_2 itself at the sediment surface of Lake Tantaré
596 Basin A. Indeed, the sediment surface was also oxic at the sites Melide and Figino of Lake

Lugano in March 1989 (Table 4) as revealed by detectable bottom water [O_2] (Table 4), and by low [Fe], undetectable ΣS(−II) and [CH_4] and relatively high [SO_4^{2-}] in overlying water (Lazzaretti et al., 1992; Lazzaretti-Ulmer and Hanselmann, 1999). Despite this, the COS values determined for the two sites of Lake Lugano appear to be realistic and coherent with those calculated for Lakes Tantaré Basin B, Bédard and Jacks. However, we know that benthic organisms are present in Lake Tantaré Basin A (Hare et al., 1994) but lacking at the two sites of Lake Lugano, as shown by the presence of varves (Span et al., 1992) and the absence of benthos remains in the recent sediments at these sites (Niessen et al., 1992). Clayer et al. (2016) provided evidences that sediment irrigation by benthic animals is effective in Lake Tantaré Basin A and that it should be taken into account in modeling the porewater solutes profiles. However, these authors also point out the difficulty to properly estimate the magnitude of solute transport by bioirrigation. The term used in Eq. 2 to calculate this contribution, i.e., $\varphi\alpha_{irrigation}$ ($[solute]_{tube}$ − [solute]), is indeed an approximation of intricate 3-D processes (Meile et al. 2005). And, in the conceptualization of this bioirrigation term, it was notably assumed that benthic animals continuously irrigate their tubes to maintain solute concentrations in their biogenic structures ($[solute]_{tube}$) identical to those in the water overlying the sediments. But microbenthic animals are generally reported to irrigate the sediments in a discontinuous manner and the solute concentrations in their biogenic structures may be highly variable with time (Boudreau and Marinelli 1994; Forster and Graf 1995; Riisgård and Larsen 2005; Gallon et al. 2008). Hence, owing to the imperfection of the representation of bioirrigation in Eq. 2, COS values estimated for the sediment of Lake Tantaré Basin A should be treated with caution, especially in the Z_1 where the bioirrigation coefficient takes the highest value. Another potential bias in the estimation of COS values for the oxygenated basin is the possibility of DIC production through HMW OM fermentation (reaction r2; Corbett et al. 2013). Note that fitting with Eq. 6 the experimental $\delta^{13}C$ data does not allow partitioning the production of DIC between r1 and r2 since the two processes share the same value of fractionation factor ($\alpha_1 = \alpha_1 = 1.000$). It was possible to attribute unequivocally the excess of DIC production rate over that of CH_4 production in the Z_2 of Lake Bédard in October 2015 (Table 4 and Section S2.1.2.2 of the SI) to HMW OM fermentation merely because R_{net}^{Ox} was negligible compared to $R_{net}^{CH_4}$ and R_{net}^{DIC}, which is not the case for Lake Tantaré Basin A (Table 4). Equation 12 indicates that to obtain negative COS values for Lake Tantaré Basin A in September 2006 and October 2005, R_2 should be >11 fmol

628 cm^{-2} s^{-1} and >110 fmol cm^{-2} s^{-1}, respectively. These R_2 values correspond to transferring >9%
629 and >44% of the rate of DIC production from R_1 to R_2 for September 2006 and October 2005,
630 respectively. The above discussion underlines several factors that can explain the unreliability in
631 the actual COS estimation for the perennially oxic Lake Tantaré Basin A, and further research is
632 needed to better assess the importance of these factors. However, it does not dismiss that the
633 substrate for methanogenesis in this lake basin may have a negative COS value.

634 **5 Conclusions**

635 Our results show that fermentation and methanogenesis represent nearly 50% and 100%
636 of OM mineralization in the top 25 cm of the sediments at the hypolimnetic sites in Lake Bédard
637 and in Basin A of Lake Tantaré, respectively and that methane is produced only by
638 hydrogenotrophy at these two sites. An earlier study reached similar conclusions about the
639 pathways of methanogenesis and the contribution of this process in OM mineralization in Basin
640 B of Lake Tantaré (Clayer et al. 2018).

641 Reactive-transport modelling of porewater solutes from three boreal lakes, i.e., Bédard,
642 Tantaré (Basin B) and Jacks, as well as of the sub-alpine Lake Lugano (Melide and Figino sites)
643 consistently showed that the main substrates for sediment methanogenesis at deep seasonally
644 anoxic hypolimnetic sites have a mean COS value of -1.4 ± 0.3. Mineralization of the most
645 labile compounds during OM downward migration in the water column and in the uppermost
646 sediment layers likely explains why reduced organic compounds fuel methanogenesis in these
647 sediments.

648 The current representation of the fermenting OM, i.e., CH_2O, in process-based
649 biogeochemical models entails a significant risk of misestimating sedimentary CH_4 and CO_2
650 production and release to the bottom water and, to a certain extent, of mispredicting evasion of
651 these greenhouse gases to the atmosphere under transient environmental scenarios. To better
652 constrain CH_4 and CO_2 production within sediments, we suggest taking specifically into account
653 the COS of the fermenting OM in formulating the reactions of methanogenesis associated with
654 fermentation in these models. For example, the rates of CH_4 (R^{CH_4}) and DIC (R^{DIC}) production
655 during fermentation coupled to hydrogenotrophy can be expressed as:

$$R^{CH_4} = R_4 = \frac{4 - COS}{8} R_1 \quad (13)$$

$$R^{DIC} = R_1 - R_4 = R_1 \left(1 - \frac{4 - COS}{8}\right) \quad (14)$$

Given these rate expressions, the stoichiometric formulation of a typical fermentation reaction producing methane becomes:

$$CH_a O_b \rightarrow \frac{4 - COS}{8} CH_4 + \left(\frac{4 + COS}{8}\right) CO_2 \quad (15)$$

where $a = 2 - \frac{COS}{2}$, $b = 1 + \frac{COS}{4}$. Note that the same stoichiometric formulation would be obtained for acetoclastic methanogenesis.

The approach used to estimate the COS of the fermenting OM, although successful for the seasonally anoxic basins, failed to produce reliable COS values when applied to the perennially oxygenated Basin A of Lake Tantaré. We attribute this peculiarity to a misestimation and/or misrepresentation of the benthic irrigation and to the impossibility to partition the DIC production between reactions r1 and r2 which share the same fractionation factor value. Similar problems would likely be encountered also in other lake ecosystems such as epilimnetic sediments and wetlands where solute transport processes remain ill-known. Indeed, these shallow aquatic environments are subject to enhanced benthic activity (Hare 1995), to plant-mediated transport of CH_4 and O_2 (Chanton et al. 1989; Wang et al. 2006), as well as to turbulence (Poindexter et al. 2016) which complicates the estimation of CH_4 and CO_2 production and consumption rates. Hence, the remaining challenge resides in the robust estimations the COS of the fermenting OM in epilimnetic sediments and shallow freshwater environments (e.g., ponds, wetlands), since these environments were shown to be the main contributors to freshwater CH_4 release to the atmosphere (Del Sontro et al., 2016, Bastviken et al., 2008). One potential solution is to investigate trends in the oxygen isotope signatures in the sedimentary DIC in addition to $\delta^{13}C$ values since it is also influenced by the source of the OM undergoing degradation (e.g., Sauer et al., 2001).

Acknowledgments, Samples, and Data

We thank P. Boissinot, L. Rancourt, P. Girard, J.-F. Dutil, S. Duval, A. Royer-Lavallée, A. Laberge and A. Barber for research and field work assistance. We are also thankful to J.-F. Hélie, from the Laboratoire de géochimie des isotopes stables légers (UQÀM), who graciously calibrated our $\delta^{13}C$ internal standard. This work was supported by grants to C.G., A.T. and Y.G. from the Natural Sciences and Engineering Research Council of Canada and the Fonds de Recherche Québécois – Nature et Technologies. Permission from the Québec Ministère du Développement durable, de l'Environnement et de la Lutte contre les changements climatiques to work in the Tantaré Ecological Reserve is gratefully acknowledged.

Data access: Upon acceptance, readers will be able to access the data at this url: https://www.hydroshare.org/resource/38e069761d7b4cf4abe3cbcaaac06016/

References

Alperin, M. J., Albert, D. B., & Martens, C. S. (1994). Seasonal variations in production and consumption rates of dissolved organic carbon in an organic-rich coastal sediment. *Geochimica et Cosmochimica Acta*, *58*(22), 4909–4930. https://doi.org/10.1016/0016-7037(94)90221-6

Alperin, M. J., Reeburgh, W. S., & Whiticar, M. J. (1988). Carbon and hydrogen isotope fractionation resulting from anaerobic methane oxidation. *Global Biogeochemical Cycles*, *2*(3), 279–288. https://doi.org/10.1029/GB002i003p00279

Arndt, S., Jørgensen, B. B., LaRowe, D. E., Middelburg, J. J., Pancost, R. D., & Regnier, P. (2013). Quantifying the degradation of organic matter in marine sediments: A review and synthesis. *Earth-Science Reviews*, *123*, 53–86. https://doi.org/10.1016/j.earscirev.2013.02.008

Arning, E. T., van Berk, W., & Schulz, H.-M. (2016). Fate and behaviour of marine organic matter during burial of anoxic sediments: Testing CH2O as generalized input parameter in reaction transport models. *Marine Chemistry*, *178*, 8–21. https://doi.org/10.1016/j.marchem.2015.12.002

Barbieri, A., & Mosello, R. (1992). Chemistry and trophic evolution of Lake Lugano in relation to nutrient budget. *Aquatic Sciences*, *54*(3), 219–237. https://doi.org/10.1007/BF00878138

Bastviken, D., Cole, J. J., Pace, M. L., & Van de Bogert, M. C. (2008). Fates of methane from different lake habitats: Connecting whole-lake budgets and CH_4 emissions. *Journal of Geophysical Research: Biogeosciences*, *113*(G2). https://doi.org/10.1029/2007JG000608

Bastviken, D., Cole, J., Pace, M., & Tranvik, L. (2004). Methane emissions from lakes: Dependence of lake characteristics, two regional assessments, and a global estimate. *Global Biogeochemical Cycles*, *18*(4). https://doi.org/10.1029/2004GB002238

Beal, E. J., House, C. H., & Orphan, V. J. (2009). Manganese- and iron-dependent marine methane oxidation. *Science (New York, N.Y.)*, *325*(5937), 184–187. https://doi.org/10.1126/science.1169984

Berg, P., Risgaard-Petersen, N., & Rysgaard, S. (1998). Interpretation of measured concentration profiles in sediment pore water. *Limnology and Oceanography*, *43*(7), 1500–1510. https://doi.org/10.4319/lo.1998.43.7.1500

Blair, N. E., & Carter, W. D. (1992). The carbon isotope biogeochemistry of acetate from a methanogenic marine sediment. *Geochimica et Cosmochimica Acta*, *56*(3), 1247–1258. https://doi.org/10.1016/0016-7037(92)90060-V

Borowski, W. S., Paull, C. K., & Ussler, W. (1997). Carbon cycling within the upper methanogenic zone of continental rise sediments; An example from the methane-rich sediments overlying the Blake Ridge gas hydrate deposits. *Marine Chemistry*, *57*(3), 299–311. https://doi.org/10.1016/S0304-4203(97)00019-4

Bottinga, Y. (1969). Calculated fractionation factors for carbon and hydrogen isotope exchange in the system calcite-carbon dioxide-graphite-methane-hydrogen-water vapor. *Geochimica et Cosmochimica Acta*, *33*(1), 49–64. https://doi.org/10.1016/0016-7037(69)90092-1

Boudreau, B., & Marinelli, R. (1994). A modeling study of discontinuous biological irrigation. *Journal of Marine Research*, *52*, 947–968. https://doi.org/10.1357/0022240943076902

Boudreau, B. P. (1997). *Diagenetic models and their implementation: modelling transport and reactions in aquatic sediments*. Springer.

Burdige, D. J. (2007). Preservation of Organic Matter in Marine Sediments: Controls, Mechanisms, and an Imbalance in Sediment Organic Carbon Budgets? *Chemical Reviews*, *107*(2), 467–485. https://doi.org/10.1021/cr050347q

Burdige, D. J., & Komada, T. (2011). Anaerobic oxidation of methane and the stoichiometry of remineralization processes in continental margin sediments. *Limnology and Oceanography*, *56*(5), 1781–1796. https://doi.org/10.4319/lo.2011.56.5.1781

Burdige, D., Komada, T., Magen, C., & Chanton, J. P. (2017). Methane dynamics in Santa Barbara Basin (USA) sediments as examined with a reaction-transport model. *Journal of Marine Research*, *74*, 277–313.

Carignan, R., & Lean, D. R. S. (1991). Regeneration of dissolved substances in a seasonally anoxic lake: The relative importance of processes occurring in the water column and in the sediments. *Limnology and Oceanography*, *36*(4), 683–707. https://doi.org/10.4319/lo.1991.36.4.0683

Carignan, R., Rapin, F., & Tessier, A. (1985). Sediment porewater sampling for metal analysis: A comparison of techniques. *Geochimica et Cosmochimica Acta*, *49*(11), 2493–2497. https://doi.org/10.1016/0016-7037(85)90248-0

Carmichael, M. J., Bernhardt, E. S., Bräuer, S. L., & Smith, W. K. (2014). The role of vegetation in methane flux to the atmosphere: should vegetation be included as a distinct category in the global methane budget? *Biogeochemistry*, *119*(1), 1–24. https://doi.org/10.1007/s10533-014-9974-1

Chanton, J. P., Whiting, G. J., Blair, N. E., Lindau, C. W., & Bollich, P. K. (1997). Methane emission from rice: Stable isotopes, diurnal variations, and CO2 exchange. *Global Biogeochemical Cycles*, *11*(1), 15–27. https://doi.org/10.1029/96GB03761

Chanton, J. P., Martens, C. S., & Kelley, C. A. (1989). Gas transport from methane-saturated, tidal freshwater and wetland sediments. *Limnology and Oceanography*, *34*(5), 807–819. https://doi.org/10.4319/lo.1989.34.5.0807

Chasar, L. S., Chanton, J. P., Glaser, P. H., Siegel, D. I., & Rivers, J. S. (2000). Radiocarbon and stable carbon isotopic evidence for transport and transformation of dissolved organic carbon, dissolved inorganic carbon, and CH4 in a northern Minnesota peatland. *Global Biogeochemical Cycles*, *14*(4), 1095–1108. https://doi.org/10.1029/1999GB001221

Clayer, F., Moritz, A., Gelinas, Y., Tessier, A., & Gobeil, C. (2018). Modeling the carbon isotope signatures of methane and dissolved inorganic carbon to unravel mineralization pathways

762 in boreal lake sediments. *Geochimica Et Cosmochimica Acta*, *229*, 36–52.
763 https://doi.org/10.1016/j.gca.2018.02.012

764 Clayer, F., Gobeil, C., & Tessier, A. (2016). Rates and pathways of sedimentary organic matter
765 mineralization in two basins of a boreal lake: Emphasis on methanogenesis and methanotrophy:
766 Methane cycling in boreal lake sediments. *Limnology and Oceanography*, *61*(S1), S131–S149.
767 https://doi.org/10.1002/lno.10323

768 Cole, J. J., Prairie, Y. T., Caraco, N. F., McDowell, W. H., Tranvik, L. J., Striegl, R. G., et al.
769 (2007). Plumbing the Global Carbon Cycle: Integrating Inland Waters into the Terrestrial Carbon
770 Budget. *Ecosystems*, *10*(1), 172–185. https://doi.org/10.1007/s10021-006-9013-8

771 Conrad, R. (1999). Contribution of hydrogen to methane production and control of hydrogen
772 concentrations in methanogenic soils and sediments. *FEMS Microbiology Ecology*, *28*(3), 193–
773 202. https://doi.org/10.1111/j.1574-6941.1999.tb00575.x

774 Conrad, R., Claus, P., Chidthaisong, A., Lu, Y., Fernandez Scavino, A., Liu, Y., et al. (2014).
775 Stable carbon isotope biogeochemistry of propionate and acetate in methanogenic soils and lake
776 sediments. *Organic Geochemistry*, *73*, 1–7. https://doi.org/10.1016/j.orggeochem.2014.03.010

777 Conrad, R. (2005). Quantification of methanogenic pathways using stable carbon isotopic
778 signatures: a review and a proposal. *Organic Geochemistry*, *36*(5), 739–752.
779 https://doi.org/10.1016/j.orggeochem.2004.09.006

780 Conrad, R, Chan, O.-C., Claus, P., & Casper, P. (2007). Characterization of methanogenic
781 Archaea and stable isotope fractionation during methane production in the profundal sediment of
782 an oligotrophic lake (Lake Stechlin, Germany). *Limnology and Oceanography*, *52*(4), 1393–
783 1406. https://doi.org/10.4319/lo.2007.52.4.1393

784 Conrad, R, Claus, P., & Casper, P. (2009). Characterization of stable isotope fractionation during
785 methane production in the sediment of a eutrophic lake, Lake Dagow, Germany. *Limnology and*
786 *Oceanography*, *54*(2), 457–471. https://doi.org/10.4319/lo.2009.54.2.0457

787 Conrad, R, Klose, M., Yuan, Q., Lu, Y., & Chidthaisong, A. (2012). Stable carbon isotope
788 fractionation, carbon flux partitioning and priming effects in anoxic soils during methanogenic
789 degradation of straw and soil organic matter. *Soil Biology and Biochemistry*, *49*, 193–199.
790 https://doi.org/10.1016/j.soilbio.2012.02.030

Corbett, J. E., Tfaily, M. M., Burdige, D. J., Cooper, W. T., Glaser, P. H., & Chanton, J. P. (2013). Partitioning pathways of CO_2 production in peatlands with stable carbon isotopes. *Biogeochemistry*, *114*, 327–340. Retrieved from JSTOR.

Corbett, J. E., Tfaily, M. M., Burdige, D. J., Glaser, P. H., & Chanton, J. P. (2015). The relative importance of methanogenesis in the decomposition of organic matter in northern peatlands. *Journal of Geophysical Research: Biogeosciences*, *120*(2), 280–293. https://doi.org/10.1002/2014JG002797

Couture, R.-M., Fischer, R., Van Cappellen, P., & Gobeil, C. (2016). Non-steady state diagenesis of organic and inorganic sulfur in lake sediments. *Geochimica et Cosmochimica Acta*, *194*, 15–33. https://doi.org/10.1016/j.gca.2016.08.029

Couture, R.-M., Gobeil, C., & Tessier, A. (2008). Chronology of Atmospheric Deposition of Arsenic Inferred from Reconstructed Sedimentary Records. *Environmental Science & Technology*, *42*(17), 6508–6513. https://doi.org/10.1021/es800818j

Cranwell, P. A. (1981). Diagenesis of free and bound lipids in terrestrial detritus deposited in a lacustrine sediment. *Organic Geochemistry*, *3*(3), 79–89. https://doi.org/10.1016/0146-6380(81)90002-4

D'arcy, P. (1993). *Relations entre les propriétés du bassin versant, la morphométrie du lac et la qualité des eaux*. INRS-ETE, Université du Québec, Québec City, Québec, Canada.

DelSontro, T., Boutet, L., St-Pierre, A., del Giorgio, P. A., & Prairie, Y. T. (2016). Methane ebullition and diffusion from northern ponds and lakes regulated by the interaction between temperature and system productivity: Productivity regulates methane lake flux. *Limnology and Oceanography*, *61*(S1), S62–S77. https://doi.org/10.1002/lno.10335

Duan, Z., & Mao, S. (2006). A thermodynamic model for calculating methane solubility, density and gas phase composition of methane-bearing aqueous fluids from 273 to 523K and from 1 to 2000bar. *Geochimica et Cosmochimica Acta*, *70*(13), 3369–3386. https://doi.org/10.1016/j.gca.2006.03.018

Egger, M., Rasigraf, O., Sapart, C. J., Jilbert, T., Jetten, M. S. M., Röckmann, T., et al. (2015). Iron-Mediated Anaerobic Oxidation of Methane in Brackish Coastal Sediments. *Environmental Science & Technology*, *49*(1), 277–283. https://doi.org/10.1021/es503663z

Emrich, K., Ehhalt, D. H., & Vogel, J. C. (1970). Carbon isotope fractionation during the precipitation of calcium carbonate. *Earth and Planetary Science Letters*, *8*(5), 363–371. https://doi.org/10.1016/0012-821X(70)90109-3

Ettwig, K. F., Butler, M. K., Le Paslier, D., Pelletier, E., Mangenot, S., Kuypers, M. M. M., et al. (2010). Nitrite-driven anaerobic methane oxidation by oxygenic bacteria. *Nature*, *464*(7288), 543–548. https://doi.org/10.1038/nature08883

Feyte, S., Gobeil, C., Tessier, A., & Cossa, D. (2012). Mercury dynamics in lake sediments. *Geochimica et Cosmochimica Acta*, *82*, 92–112. https://doi.org/10.1016/j.gca.2011.02.007

Forster, S., & Graf, G. (1995). Impact of irrigation on oxygen flux into the sediment: intermittent pumping by Callianassa subterranea and "piston-pumping" by Lanice conchilega. *Marine Biology*, *123*(2), 335–346. https://doi.org/10.1007/BF00353625

Galand, P. E., Yrjälä, K., & Conrad, R. (2010). Stable carbon isotope fractionation during methanogenesis in three boreal peatland ecosystems. *Biogeosciences*, *7*(11), 3893–3900. https://doi.org/10.5194/bg-7-3893-2010

Gallon, C., Hare, L., & Tessier, A. (2008). Surviving in anoxic surroundings: how burrowing aquatic insects create an oxic microhabitat. *Journal of the North American Benthological Society*, *27*(3), 570–580. https://doi.org/10.1899/07-132.1

Gelwicks, J. T., Risatti, J. B., & Hayes, J. M. (1994). Carbon isotope effects associated with aceticlastic methanogenesis. *Applied and Environmental Microbiology*, *60*(2), 467–472.

Ghosh, P., & Brand, W. A. (2003). Stable isotope ratio mass spectrometry in global climate change research. *International Journal of Mass Spectrometry*, *228*(1), 1–33. https://doi.org/10.1016/S1387-3806(03)00289-6

Gobeil, C., Tessier, A., & Couture, R.-M. (2013). Upper Mississippi Pb as a mid-1800s chronostratigraphic marker in sediments from seasonally anoxic lakes in Eastern Canada. *Geochimica et Cosmochimica Acta*, *113*, 125–135. https://doi.org/10.1016/j.gca.2013.02.023

Happell, J. D., Chanton, J. P., & Showers, W. J. (1995). Methane transfer across the water-air interface in stagnant wooded swamps of Florida: Evaluation of mass-transfer coefficients and isotropic fractionation. *Limnology and Oceanography*, *40*(2), 290–298. https://doi.org/10.4319/lo.1995.40.2.0290

Hare, L. (1995). Sediment Colonization by Littoral and Profundal Insects. *Journal of the North American Benthological Society*, *14*, 315. https://doi.org/10.2307/1467783

Hare, L., Carignan, R., & Huerta-Diaz, M. A. (1994). A field study of metal toxicity and accumulation by benthic invertebrates; implications for the acid-volatile sulfide (AVS) model. *Limnology and Oceanography*, *39*(7), 1653–1668. https://doi.org/10.4319/lo.1994.39.7.1653

Hastie, A., Lauerwald, R., Weyhenmeyer, G., Sobek, S., Verpoorter, C., & Regnier, P. (2018). CO_2 evasion from boreal lakes: Revised estimate, drivers of spatial variability, and future projections. *Global Change Biology*, *24*(2), 711–728. https://doi.org/10.1111/gcb.13902

Hedges, J. I., & Oades, J. M. (1997). Comparative organic geochemistries of soils and marine sediments. *Organic Geochemistry*, *27*(7), 319–361. https://doi.org/10.1016/S0146-6380(97)00056-9

Hélie, J.-F. (2004). *Géochimie et flux de carbone organique et inorganique dans les milieux aquatiques de l'est du Canada : exemples du Saint-Laurent et du réservoir Robert-Bourassa : approche isotopique* (Phd, Université du Québec à Chicoutimi .). Retrieved from https://constellation.uqac.ca/672/

Hesslein, R. H. (1976). An in situ sampler for close interval pore water studies1. *Limnology and Oceanography*, *21*(6), 912–914. https://doi.org/10.4319/lo.1976.21.6.0912

Holgerson, M. A., & Raymond, P. A. (2016). Large contribution to inland water CO2 and CH4 emissions from very small ponds. *Nature Geoscience*, *9*(3), 222–226. https://doi.org/10.1038/ngeo2654

Holmkvist, L., Ferdelman, T. G., & Jørgensen, B. B. (2011). A cryptic sulfur cycle driven by iron in the methane zone of marine sediment (Aarhus Bay, Denmark). *Geochimica et Cosmochimica Acta*, *75*(12), 3581–3599. https://doi.org/10.1016/j.gca.2011.03.033

Hornibrook, E. R. C., Longstaffe, F. J., & Fyfe, W. S. (1997). Spatial distribution of microbial methane production pathways in temperate zone wetland soils: Stable carbon and hydrogen isotope evidence. *Geochimica et Cosmochimica Acta*, *61*(4), 745–753. https://doi.org/10.1016/S0016-7037(96)00368-7

Hornibrook, E. R. C., Longstaffe, F. J., & Fyfe, W. S. (2000). Evolution of stable carbon isotope compositions for methane and carbon dioxide in freshwater wetlands and other anaerobic

environments. *Geochimica et Cosmochimica Acta*, *64*(6), 1013–1027. https://doi.org/10.1016/S0016-7037(99)00321-X

Jähne, B., Heinz, G., & Dietrich, W. (1987). Measurement of the diffusion coefficients of sparingly soluble gases in water. *Journal of Geophysical Research: Oceans*, *92*(C10), 10767–10776. https://doi.org/10.1029/JC092iC10p10767

Jørgensen, B. B., & Parkes, R. J. (2010). Role of sulfate reduction and methane production by organic carbon degradation in eutrophic fjord sediments (Limfjorden, Denmark). *Limnology and Oceanography*, *55*(3), 1338–1352. https://doi.org/10.4319/lo.2010.55.3.1338

Joshani, A. (2015). *Investigating organic matter preservation through complexation with iron oxides in Lake Tantaré* (Masters, Concordia University). Retrieved from https://spectrum.library.concordia.ca/980434/

Kankaala, P., Huotari, J., Tulonen, T., & Ojala, A. (2013). Lake-size dependent physical forcing drives carbon dioxide and methane effluxes from lakes in a boreal landscape. *Limnology and Oceanography*, *58*(6), 1915–1930. https://doi.org/10.4319/lo.2013.58.6.1915

Krzycki, J. A., Kenealy, W. R., DeNiro, M. J., & Zeikus, J. G. (1987). Stable Carbon Isotope Fractionation by Methanosarcina barkeri during Methanogenesis from Acetate, Methanol, or Carbon Dioxide-Hydrogen. *Applied and Environmental Microbiology*, *53*(10), 2597–2599.

Laforte, L., Tessier, A., Gobeil, C., & Carignan, R. (2005). Thallium diagenesis in lacustrine sediments. *Geochimica et Cosmochimica Acta*, *69*(22), 5295–5306. https://doi.org/10.1016/j.gca.2005.06.006

Lapham, L., Proctor, L., & Chanton, J. (1999). Using Respiration Rates and Stable Carbon Isotopes to Monitor the Biodegradation of Orimulsion by Marine Benthic Bacteria. *Environmental Science & Technology*, *33*(12), 2035–2039. https://doi.org/10.1021/es981158a

LaRowe, D. E., & Van Cappellen, P. (2011). Degradation of natural organic matter: A thermodynamic analysis. *Geochimica et Cosmochimica Acta*, *75*(8), 2030–2042. https://doi.org/10.1016/j.gca.2011.01.020

Lazzaretti, M. A., Hanselmann, K. W., Brandl, H., Span, D., & Bachofen, R. (1992). The role of sediments in the phosphorus cycle in Lake Lugano. II. Seasonal and spatial variability of

906 microbiological processes at the sediment-water interface. *Aquatic Sciences*, *54*(3), 285–299.
907 https://doi.org/10.1007/BF00878142

908 Lazzaretti-Ulmer, M. A., & Hanselmann, K. W. (1999). Seasonal variation of the microbially
909 regulated buffering capacity at sediment-water interfaces in a freshwater lake. *Aquatic Sciences*,
910 *61*(1), 59–74. https://doi.org/10.1007/s000270050052

911 Lettmann, K. A., Riedinger, N., Ramlau, R., Knab, N., Böttcher, M. E., Khalili, A., et al. (2012).
912 Estimation of biogeochemical rates from concentration profiles: A novel inverse method.
913 *Estuarine, Coastal and Shelf Science*, *100*, 26–37. https://doi.org/10.1016/j.ecss.2011.01.012

914 Matsumoto, G. I. (1989). Biogeochemical study of organic substances in Antarctic lakes.
915 *Hydrobiologia*, *172*(1), 265–299. https://doi.org/10.1007/BF00031627

916 Meile, C. D., Berg, P., Cappellen, P. S. J., & Tuncay, K. (2005). Solute-specific pore water
917 irrigation: Implications for chemical cycling in early diagenesis. *Journal of Marine Research*, *63*.
918 https://doi.org/10.1357/0022240054307885

919 Mook, W. G., Bommerson, J. C., & Staverman, W. H. (1974). Carbon isotope fractionation
920 between dissolved bicarbonate and gaseous carbon dioxide. *Earth and Planetary Science Letters*,
921 *22*(2), 169–176. https://doi.org/10.1016/0012-821X(74)90078-8

922 Natchimuthu, S., Wallin, M. B., Klemedtsson, L., & Bastviken, D. (2017). Spatio-temporal
923 patterns of stream methane and carbon dioxide emissions in a hemiboreal catchment in
924 Southwest Sweden. *Scientific Reports*, *7*(1). https://doi.org/10.1038/srep39729

925 Niessen, F., Wick, L., Bonani, G., Chondrogianni, C., & Siegenthaler, C. (1992). Aquatic system
926 response to climatic and human changes: Productivity, bottom water oxygen status, and sapropel
927 formation in Lake Lugano over the last 10 000 years. *Aquatic Sciences*, *54*(3), 257–276.
928 https://doi.org/10.1007/BF00878140

929 Norði, K., Thamdrup, B., & Schubert, C. J. (2013). Anaerobic oxidation of methane in an iron-
930 rich Danish freshwater lake sediment. *Limnology and Oceanography*, *58*(2), 546–554.
931 https://doi.org/10.4319/lo.2013.58.2.0546

932 O'Leary, M. H. (1984). Measurement of the isotope fractionation associated with diffusion of
933 carbon dioxide in aqueous solution. *The Journal of Physical Chemistry*, *88*(4), 823–825.
934 https://doi.org/10.1021/j150648a041

Paraska, D. W., Hipsey, M. R., & Salmon, S. U. (2014). Sediment diagenesis models: Review of approaches, challenges and opportunities. *Environmental Modelling & Software*, *61*, 297–325. https://doi.org/10.1016/j.envsoft.2014.05.011

Pick, F. R., Lean, D. R. S., & Nalewajko, C. (1984). Nutrient status of metalimnetic phytoplankton peaks. *Limnology and Oceanography*, *29*(5), 960–971. https://doi.org/10.4319/lo.1984.29.5.0960

Pohlman, J. W., Ruppel, C., Hutchinson, D. R., Downer, R., & Coffin, R. B. (2008). Assessing sulfate reduction and methane cycling in a high salinity pore water system in the northern Gulf of Mexico. *Marine and Petroleum Geology*, *25*(9), 942–951. https://doi.org/10.1016/j.marpetgeo.2008.01.016

Pohlman, John W., Riedel, M., Bauer, J. E., Canuel, E. A., Paull, C. K., Lapham, L., et al. (2013). Anaerobic methane oxidation in low-organic content methane seep sediments. *Geochimica et Cosmochimica Acta*, *108*, 184–201. https://doi.org/10.1016/j.gca.2013.01.022

Poindexter, C. M., Baldocchi, D. D., Matthes, J. H., Knox, S. H., & Variano, E. A. (2016). The contribution of an overlooked transport process to a wetland's methane emissions. *Geophysical Research Letters*, *43*(12), 6276–6284. https://doi.org/10.1002/2016GL068782

Raghoebarsing, A. A., Pol, A., van de Pas-Schoonen, K. T., Smolders, A. J. P., Ettwig, K. F., Rijpstra, W. I. C., et al. (2006). A microbial consortium couples anaerobic methane oxidation to denitrification. *Nature*, *440*(7086), 918–921. https://doi.org/10.1038/nature04617

Riisgård, H. U., & Larsen, P. S. (2005). Water pumping and analysis of flow in burrowing zoobenthos: an overview. *Aquatic Ecology*, *39*(2), 237–258. https://doi.org/10.1007/s10452-004-1916-x

Sabrekov, A. F., Runkle, B. R. K., Glagolev, M. V., Terentieva, I. E., Stepanenko, V. M., Kotsyurbenko, O. R., et al. (2017). Variability in methane emissions from West Siberia's shallow boreal lakes on a regional scale and its environmental controls. *Biogeosciences*, *14*(15), 3715–3742. https://doi.org/10.5194/bg-14-3715-2017

Sauer, P. E., Miller, G. H., & Overpeck, J. T. (2001). Oxygen isotope ratios of organic matter in arctic lakes as a paleoclimate proxy: field and laboratory investigations. *Journal of Paleolimnology*, *25*(1), 43–64. https://doi.org/10.1023/A:1008133523139

964 Saunois, M., Bousquet, P., Poulter, B., Peregon, A., Ciais, P., Canadell, J. G., et al. (2016). The
965 global methane budget 2000–2012. *Earth System Science Data*, *8*(2), 697–751.
966 https://doi.org/10.5194/essd-8-697-2016

967 Schindler, D. W., Curtis, P. J., Parker, B. R., & Stainton, M. P. (1996). Consequences of climate
968 warming and lake acidification for UV-B penetration in North American boreal lakes. *Nature*,
969 *379*(6567), 705–708. https://doi.org/10.1038/379705a0

970 Sivan, O., Schrag, D. P., & Murray, R. W. (2007). Rates of methanogenesis and methanotrophy
971 in deep-sea sediments. *Geobiology*, *5*(2), 141–151. https://doi.org/10.1111/j.1472-
972 4669.2007.00098.x

973 Span, D., Dominik, J., Lazzaretti, M. A., & Vernet, J.-P. (1992). The role of sediments in the
974 phosphorus cycle in Lake Lugano. I. Geochemical approach. *Aquatic Sciences*, *54*(3), 277–284.
975 https://doi.org/10.1007/BF00878141

976 Staehr, P. A., Testa, J. M., Kemp, W. M., Cole, J. J., Sand-Jensen, K., & Smith, S. V. (2012).
977 The metabolism of aquatic ecosystems: history, applications, and future challenges. *Aquatic*
978 *Sciences*, *74*(1), 15–29. https://doi.org/10.1007/s00027-011-0199-2

979 Thottathil, S. D., Reis, P. C. J., & Prairie, Y. T. (2019). Methane oxidation kinetics in northern
980 freshwater lakes. *Biogeochemistry*, *143*(1), 105–116. https://doi.org/10.1007/s10533-019-00552-
981 x

982 Tipping, E. (2002). *Cation binding by humic substances*. Cambridge University Press.

983 Turner, A. J., Jacob, D. J., Wecht, K. J., Maasakkers, J. D., Lundgren, E., Andrews, A. E., et al.
984 (2015). Estimating global and North American methane emissions with high spatial resolution
985 using GOSAT satellite data. *Atmospheric Chemistry and Physics*, *15*(12), 7049–7069.
986 https://doi.org/10.5194/acp-15-7049-2015

987 Ullman, W. J., & Aller, R. C. (1982). Diffusion coefficients in nearshore marine sediments1.
988 *Limnology and Oceanography*, *27*(3), 552–556. https://doi.org/10.4319/lo.1982.27.3.0552

989 Verpoorter, C., Kutser, T., Seekell, D. A., & Tranvik, L. J. (2014). A global inventory of lakes
990 based on high-resolution satellite imagery. *Geophysical Research Letters*, *41*(18), 6396–6402.
991 https://doi.org/10.1002/2014GL060641

992 Wallin, M. B., Campeau, A., Audet, J., Bastviken, D., Bishop, K., Kokic, J., et al. (2018).
993 Carbon dioxide and methane emissions of Swedish low-order streams—a national estimate and
994 lessons learnt from more than a decade of observations. *Limnology and Oceanography Letters*,
995 *3*(3), 156–167. https://doi.org/10.1002/lol2.10061

996 Wand, U., Samarkin, V. A., Nitzsche, H.-M., & Hubberten, H.-W. (2006). Biogeochemistry of
997 methane in the permanently ice-covered Lake Untersee, central Dronning Maud Land, East
998 Antarctica. *Limnology and Oceanography*, *51*(2), 1180–1194.
999 https://doi.org/10.4319/lo.2006.51.2.1180

1000 Wang, Y., & Van Cappellen, P. (1996). A multicomponent reactive transport model of early
1001 diagenesis: Application to redox cycling in coastal marine sediments. *Geochimica et*
1002 *Cosmochimica Acta*, *60*(16), 2993–3014. https://doi.org/10.1016/0016-7037(96)00140-8

1003 Werth, M., & Kuzyakov, Y. (2010). 13C fractionation at the root–microorganisms–soil interface:
1004 A review and outlook for partitioning studies. *Soil Biology and Biochemistry*, *42*(9), 1372–1384.
1005 https://doi.org/10.1016/j.soilbio.2010.04.009

1006 Whiticar, M. J, Faber, E., & Schoell, M. (1986). Biogenic methane formation in marine and
1007 freshwater environments: CO2 reduction vs. acetate fermentation—Isotope evidence.
1008 *Geochimica et Cosmochimica Acta*, *50*(5), 693–709. https://doi.org/10.1016/0016-
1009 7037(86)90346-7

1010 Whiticar, M. J. (1999). Carbon and hydrogen isotope systematics of bacterial formation and
1011 oxidation of methane. *Chemical Geology*, *161*(1), 291–314. https://doi.org/10.1016/S0009-
1012 2541(99)00092-3

1013 Whiticar, M. J., & Faber, E. (1986). Methane oxidation in sediment and water column
1014 environments—Isotope evidence. *Organic Geochemistry*, *10*(4), 759–768.
1015 https://doi.org/10.1016/S0146-6380(86)80013-4

1016 Wuebbles, D. J., & Hayhoe, K. (2002). Atmospheric methane and global change. *Earth-Science*
1017 *Reviews*, *57*(3), 177–210. https://doi.org/10.1016/S0012-8252(01)00062-9Deng, A., & Stauffer,
1018 D. R. (2006), On improving 4-km mesoscale model simulations. *Journal of Applied Meteorology*
1019 *and Climatology*, 45(3), 361–381. doi:10.1175/JAM2341.1

Global Biogeochemical Cycles

Supporting Information for

Mineralization of organic matter in boreal lake sediments: Rates, pathways and nature of the fermenting substrates

F. Clayer[a,c,*], Y. Gélinas[b,c], A. Tessier[a] and C. Gobeil[a,c]

[a] INRS-ETE, Université du Québec, 490 rue de la Couronne, Québec (QC), Canada G1K 9A9
[b] Concordia University, Department of Chemistry and Biochemistry, 7141 Sherbrooke Street West, Montreal (QC), Canada H4B 1R6
[c] Geotop, Interuniversity research and training centre in geosciences, 201 Président-Kennedy Ave., Montréal (QC), Canada H2X 3Y7
Corresponding author: François Clayer (francois.clayer@niva.no) Phone: +47 406 28 963
[*] Present address: Norwegian Institute of Water Research (NIVA), Gaustadalléen 21, 0349 Oslo, Norway

Contents of this file

Introduction

This document includes additional figures (Figures **S1** and **S2**) referred in the main article, a section describing in detail the procedure for modeling the $\delta^{13}C$ profiles (**S2**) and background information on other data from Lakes Tantaré, Bédard, Jacks and Lugano used to calculate the COS (**S3**)

S1. Additional figures

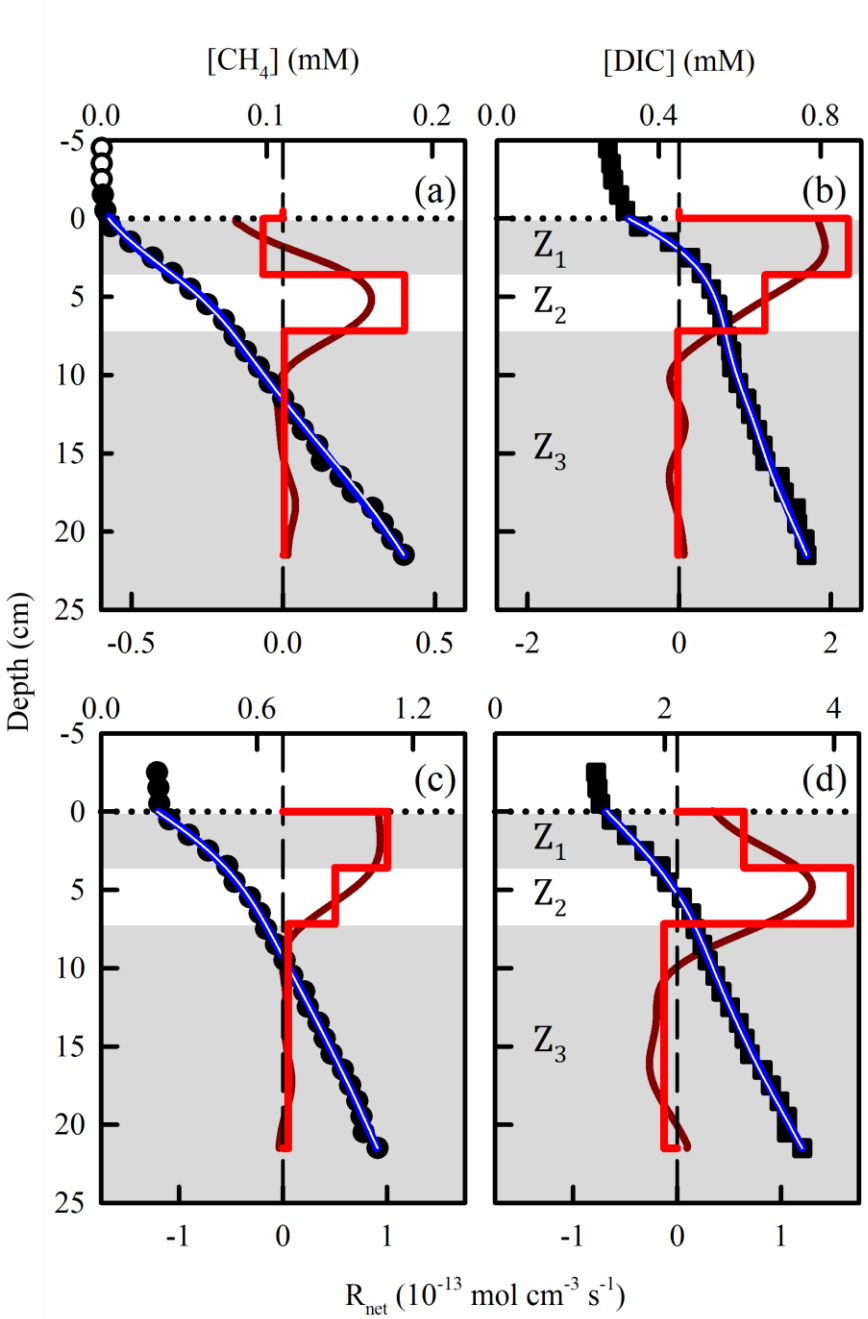

Figure S1: Comparison of concentration profiles generated with the codes PROFILE (blue line) and REC (white line) with the average (n = 3) measured concentrations (symbols) of CH_4 (a and c) and DIC (b and d) for Lake Tantaré Basin A (a and b) and Lake Bédard (c and d). The horizontal dotted line indicates the sediment-water interface. The thick red (PROFILE) and dark red (REC) lines represent the net solute reaction rate profiles.

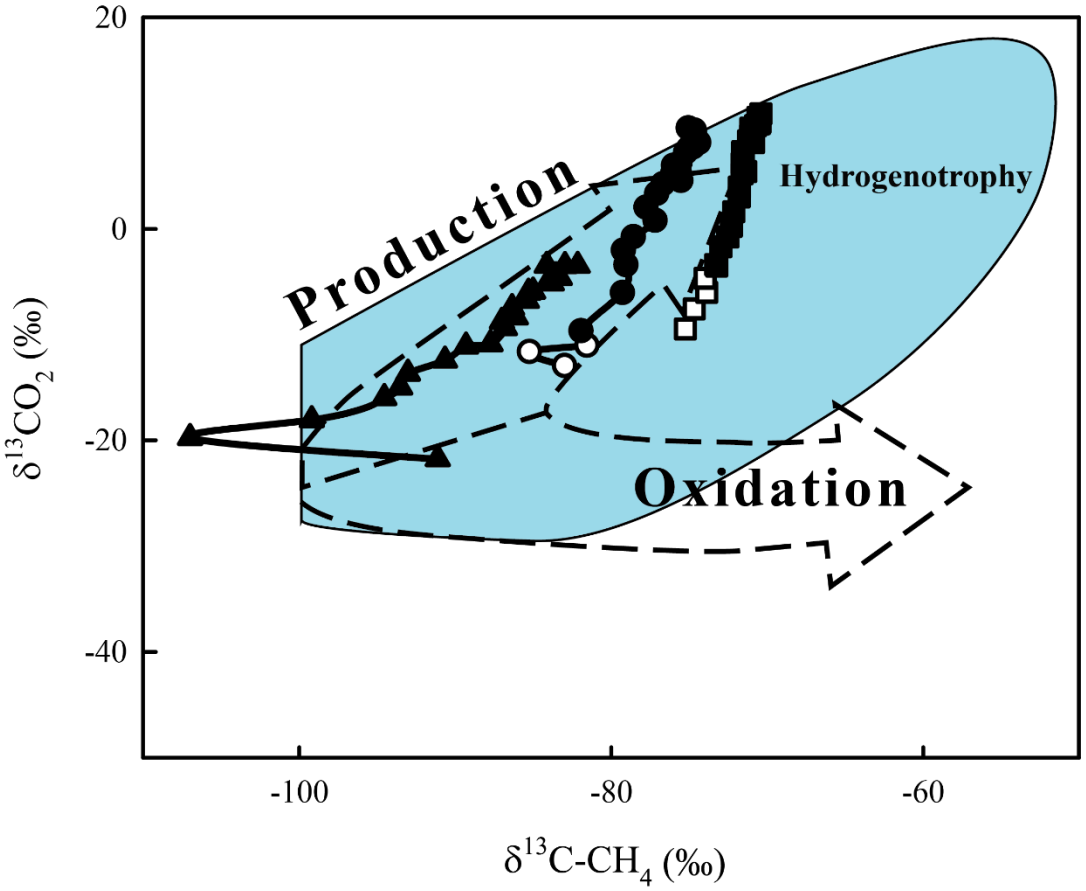

Figure S2: $\delta^{13}C$-CH_4 versus $\delta^{13}CO_2$ graph showing the hydrogenotrophy (blue) domain (modified from Whiticar 1999) along with the measured $\delta^{13}C$ data (symbols) in Lake Tantaré Basin A (triangles) and Basin B (squares; data from Clayer et al., 2018), and in Lake Bédard (circles). Empty symbols correspond to datapoints above the sediment-water interface. The $\delta^{13}C$ of gaseous CO_2 ($\delta^{13}CO_2$ on the vertical axis) was calculated from the $\delta^{13}C$-DIC according to Hélie (2004) and Mook et al. (1974).

S2. Procedure for modeling the $\delta^{13}C$ profiles

Modeling the $\delta^{13}C$ profiles with Eq. 7, as described in section 2.4, requires first obtaining accurate [C] and [^{13}C] profiles by solving numerically, via the bvp5c function of MATLAB®, Eqs. 2 and 7 for $[C]$ and $[^{13}C]$, respectively. Equation 2 is readily solved for [C] if we use in that equation the depth distributions of $R_{net}^{CH_4}$ or R_{net}^{DIC} provided by the code PROFILE (Table 2) and those of D_s and $\alpha_{Irrigation}$, and if we impose the measured CH_4 or DIC concentrations at the top and bottom of their profiles as boundary conditions. The CH_4 and DIC profiles simulated this way are very similar to those generated by the code PROFILE, and thus to the measured distributions of these two solutes. However, extracting truthful [^{13}C] profiles from Eq. 7 is more complicated because it requires obtaining the best estimate values for the parameters f, $\delta^{13}C_i^{reactant}$, α_i, and R_i which are inherent to that equation. The approach adopted to select the best estimate values involves several steps described below.

S2.1. Simulating the $\delta^{13}C$ profiles with default parameter values in Equation 7

The first step is to perform an initial simulation of the $\delta^{13}C$ profiles using credible values (hereafter referred to as default values) for the f, $\delta^{13}C_i^{reactant}$, α_i, and R_i in Eq. 7. For the f, $\delta^{13}C_i^{reactant}$ and α_i, the default values were educated guesses based on the literature. For the rates, they were R_i values constrained with Eqs. 3–5 and the $R_{net}^{CH_4}$, R_{net}^{DIC} and R_{net}^{Ox} values provided by PROFILE (Table 2).

S2.1.1. Default values for the f, $\delta^{13}C_i^{reactant}$ and α_i

The values reported in the literature for the f-CH_4 and f-DIC as well as for the $\delta^{13}C_i^{reactant}$ and the α_i of each of the r_i outlined in Table 1, are summarized in Table S1 together with the default values. The value of f–CH_4 was estimated to be less than 1.003 (Happell et al., 1995), and that of f-DIC, lower than 1.001 (O'Leary, 1984; Jähne et al., 1987). Consequently, we chose 1.000 as the default value for both. The values of $\delta^{13}C_i^{reactant}$ used were −28‰ for OM (Joshani, 2015), and −38‰ and −18‰ for the methyl and carboxyl groups of acetate (Conrad et al., 2014), respectively, and the measured $\delta^{13}C$ values for CH_4 and DIC. We assumed no carbon fractionation during OM fermentation and oxidation, i.e., $\alpha_1 = \alpha_2 = \alpha_6 = 1.000$ (Lapham et al., 1999). Methane produced through acetoclasty (r3) and hydrogenotrophy (r4) is typically depleted in ^{13}C by 21–27‰ and 50–95‰, respectively (i.e., α_3-CH_4 and α_4 ranges are 1.021–1.027 and 1.050–1.095, respectively) compared to its substrate (Krzycki et al., 1987; Gelwicks et al., 1994; Whiticar, 1999). In addition, CO_2 and CH_4 production through acetoclasty appears to undergo similar ^{13}C depletion (Blair and Carter, 1992; Gelwicks et al., 1994). Consequently, the same intermediate fractionation factor was chosen as the default value for α_3-CH_4 and α_3-CO_2, i.e., 1.024. In agreement with Conrad et al. (2014), we used 1.075 as the default value for α_4. Several studies showed that α_5 can vary from 1.005 to 1.031 (Alperin et al., 1988; Whiticar, 1999); a default value of 1.005 was selected as in Whiticar and Faber (1986). For siderite precipitation, we calculated a composite α_7 value using the fractionation factors reported for calcite precipitation from CO_2 (0.990) or from HCO_3^- (0.998) and taking into account the relative proportion of HCO_3^- and CO_2 concentrations (Bottinga, 1969; Emrich et al., 1970).

S2.1.2. Default values for the R_i

Given that methanogenesis is dominated by hydrogenotrophy (see section 3.3), and that porewaters in all sediment zones at Lake Tantaré Basin A and in the Z_1 and Z_2 at Lake Bédard are undersaturated with respect to siderite, we assume that $R_3 = R_7 = 0$ in all the zones of the two lake basins. The only exception is for the Z_3 of Lake Bédard where we infer that siderite is precipitating (see details below). In addition, we consider that $R_2 = 0$ in all the zones of the two lake basins, except in the Z_2 of Lake Bédard where reaction r2 is required to explain the DIC net production rate (see details below). The default R_i values, obtained as described below, are reported in Table S2.

Table S1: Values of the $\delta^{13}C$ of organic matter (OM), the carboxyl group (Ac-carboxyl) and the methyl group (Ac-methyl) of acetate, and those of the molecular diffusivity ratios (f) and the isotopic fractionation factors (α_i) used as input parameters in Eq. 7.

Parameters	Range	References	Default
$\delta^{13}C$ of OM (‰ V-PDB)	−28	a	−28
$\delta^{13}C$ of Ac-carboxyl (‰ V-PDB)	−18	b, c	−18
$\delta^{13}C$ of Ac-methyl (‰ V-PDB)	−38	b, c	−38
f-DIC	1.000–1.001	d, e	1.000
f-CH_4	1.000–1.003	f	1.000
α_1, α_2 and α_6	1.000	g,h,i	1.000
α_3-CH_4	1.021–1.027	j,k,l	1.024
α_3-CO_2	1.021–1.027	k,m	1.024
α_4	1.050–1.095	l,c	1.075
α_5	1.005–1.031	l,n,o	1.005
α_7	0.990–0.998	p,q	0.995

References: (a) Joshani (2015), (b) Conrad et al (2007), (c) Conrad et al. (2014), (d) O'Leary (1984), (e) Jähne et al. (1987), (f) Happell et al., 1995, (g) Lapham et al. (1999), (h) Werth and Kusyakov (2010), (i) Conrad et al. (2012), (j) Krzycki et al. (1987), (k) Gelwicks et al. (1994), (l) Whiticar (1999), (m) Blair and Carter (1992), (n) Alperin et al. (1988), (o) Whiticar and Faber (1986), (p) Bottinga (1969), (q) Emrich et al. (1970).

S2.1.2.1. Zone of net methanotrophy

According to Fig. 2g and o, net methanotrophy is observed only in the Z_1 (0–3.6 cm) of Lake Tantaré Basin A. The net rate of DIC production in that zone (223 fmol cm^{-3} s^{-1}) is much larger than the net rate of CH_4 consumption (7 fmol cm^{-3} s^{-1}) as reported in Table 2. According to Eqs. 3 and 4, the difference between the net rates of DIC and CH_4 production is:

$$R_{net}^{DIC} - R_{net}^{CH_4} = R_1 + R_2 - 2R_4 + 2R_5 + R_6 \quad \text{(S1)}.$$

Given the large net rate of oxidant consumption ($R_{net}^{Ox} = -335$ fmol cm^{-3} s^{-1}), we assume that the contribution of R_2 in Eq. S1 can be neglected compared to that of the oxidative processes ($2R_5 + R_6$). In addition, the differences between the values of the $\delta^{13}CO_2$ and those of the δ^{13}C-CH_4 (67–92‰), the large ^{13}C-CH_4 negative values (−91 to −107‰) and their upward depletion between 4.5 and 2.5 cm depth (Fig. 2b), as well as the fact that these isotopic data fall in the CO_2 reduction domain (Fig. S2), all indicate that CH_4 production by hydrogenotrophy is also active in the Z_1 of Lake Tantaré Basin A, i.e., that $R_4 \neq 0$. To simplify, we assume for now that the main oxidative process is methanotrophy and that the contribution of R_6 in Eq. S1 is negligible compared to that of $2R_5$; the effect of a possible contribution of OM oxidation to DIC will be considered in section S2.2.2.2. With the assumption that $R_2 = R_3 = R_6 = R_7 = 0$, we obtain from Eq. 3–5 the default values R_1 = 216 fmol cm^{-3} s^{-1}, R_4 = 161 fmol cm^{-3} s^{-1} and R_5 = 168 fmol cm^{-3} s^{-1}.

Table S2: Rates (R_1–R_7; fmol cm^{-3} s^{-1}) of reactions involved in OM mineralization and of siderite precipitation in each sediment zone of the two sampling sites. For each reaction rate, a default value is given and, when applicable, the range of rate values tested in modeling the $\delta^{13}C$ profiles. χ_M and χ_H are the fractions of oxidants consumed by methanotrophy and of CH_4 produced by hydrogenotrophy, respectively.

		Lake Tantaré Basin A		Lake Bédard	
Zones		Default	Range[a]	Default	Range
Z_1	R_1	216	$-105 + \chi_H(335\chi_M - 14)$	165	$-35 + 200\chi_H$
	R_2	0		0	
	R_3	0	$(1-\chi_H)\left(\frac{335}{2}\chi_M - 7\right)$	0	$100 - 100\chi_H$
	R_4	161	$\chi_H\left(\frac{335}{2}\chi_M - 7\right)$	100	$100\chi_H$
	R_5	168	$\frac{335}{2}\chi_M$	0	
	R_6	0	$335 - 335\chi_M$	0	
	R_7	0		0	
Z_2	R_1	152	$-29 + \chi_H(78 + 103\chi_M)$	100	$\frac{100\mathrm{COS}(\chi_H - 1) - 400\chi_H}{\mathrm{COS} - 4}$
	R_2	0		117	$117 + 100\chi_H - R_1$
	R_3	0	$(1-\chi_H)\left(39 + \frac{103}{2}\chi_M\right)$	0	$50 - 50\chi_H$
	R_4	90.5	$\chi_H\left(39 + \frac{103}{2}\chi_M\right)$	50	$50\chi_H$
	R_5	51.5	$\frac{103}{2}\chi_M$	0	
	R_6	0	$103 - 103\chi_M$	0	
	R_7	0		0	
Z_3	R_1	0		0	
	R_2	0		0	
	R_3	0		0	
	R_4	1		5	
	R_5	0		0	
	R_6	0		0	
	R_7	0		8	

[a]Note that χ_M cannot take values below 0.36 to avoid negative rate values for R_1 according to Equation S8.

S2.1.2.2. Zones of net methanogenesis

Figure 2g–h and Table 2 indicate that the value of the R_{net}^{DIC} (113 fmol cm^{-3} s^{-1}) is much larger than that of the $R_{net}^{CH_4}$ (39 fmol cm^{-3} s^{-1}) for the Z_2 of Lake Tantaré Basin A. Since oxidants are consumed at a substantial rate ($R_{net}^{Ox} = -103$ fmol cm^{-3} s^{-1}; Table 2), we conclude that DIC must be mainly produced through oxidation of CH_4 and/or OM (e.g., r5 and/or r6 in Table 1) in addition to fermentation (r1) and that R_2 can be neglected in Eq. S1. For now, we assume, as for the Z_1 of Lake Tantaré Basin A, that the only source of DIC in addition to fermentation (r1) is methanotrophy, and thus that $R_6 = 0$; the effect of a possible contribution of r6 to DIC will be considered in section S2.2.2.2. Thus, with the assumptions $R_2 = R_3 = R_6 = R_7 = 0$, we obtain from Eqs. 3–5 the default values R_1 = 152 fmol cm^{-3} s^{-1}, R_4 = 90.5 fmol cm^{-3} s^{-1} and R_5 = 51.5 fmol cm^{-3} s^{-1}.

Note that $R_1 > R_4$ does not necessarily mean that the sum of fermentation (r1) and methanogenesis via CO_2 reduction (r4) produces more DIC than CH_4 since the net rates of DIC and CH_4 production by the coupling of these two reactions are equal to $R_1 - R_4$ and R_4, respectively. For example, when glucose ($C_6H_{12}O_6$) is the fermenting substrate, the coupling of r1 and r4 produces equimolar amounts of CH_4 and DIC, i.e., $R_{net}^{CH_4} = R_{net}^{DIC}$, and the value of R_1 is then equal to twice that of R_4 ($R_1 = 2R_4$). The case when $R_1 < 2R_4$ is discussed in section 4 while the case when $R_1 > 2R_4$ is discussed below.

For the Z_1 of Lake Bédard, the $R_{net}^{CH_4}$ (100 fmol cm^{-3} s^{-1}) and the R_{net}^{DIC} (65 fmol cm^{-3} s^{-1}) are much larger than the R_{net}^{Ox} (−6.5 fmol cm^{-3} s^{-1}), suggesting that the reaction rates of the oxidative processes R_5 and R_6 can be neglected in these reduced sediments. Thus, if we assume that $R_2 = R_3 = R_5 = R_6 = R_7 = 0$, Eqs. 3 and 4 yield R_1 = 165 fmol cm^{-3} s^{-1} and R_4 = 100 fmol cm^{-3} s^{-1} as default values.

For the Z_2 of Lake Bédard, R_{net}^{Ox} (−4.5 fmol cm^{-3} s^{-1}) is much smaller than $R_{net}^{CH_4}$ (50 fmol cm^{-3} s^{-1}) and R_{net}^{DIC} (167 fmol cm^{-3} s^{-1}), indicating that, as in the Z_1, R_5 and R_6 can be neglected. With the assumptions that $R_3 = R_5 = R_6 = R_7 = 0$, we obtain from Eqs. 3 and 4 the default values $R_1 + R_2 = 217$ fmol cm^{-3} s^{-1} and $R_4 = 50$ fmol cm^{-3} s^{-1}. In this case DIC production rate is more than four times larger than R_4 ($R_{net}^{DIC} >> 2R_4$), which cannot be explained by methanogenesis alone or, given the low R_{net}^{Ox}, by oxidation reactions. Similar unanticipated DIC production has been previously attributed to the partial fermentation of HMW OM (r2, Corbett et al., 2015). Calculating individual default values for R_1 and R_2 requires an assumption about the nature of the fermenting substrate. For now, we assume that glucose is that substrate. i.e., that $R_1 = 2R_4$; the effect of considering more reduced fermenting substrates will be examined in section S2.2.2.3. With this latter assumption, the default values R_1 = 100 fmol cm^{-3} s^{-1} and R_2 = 117 fmol cm^{-3} s^{-1} are obtained.

Finally, in the Z_3 of each lake basin, the net DIC consumption rate (2 fmol cm^{-3} s^{-1} and 13 fmol cm^{-3} s^{-1}, for Lake Tantaré Basin A and Lake Bédard, respectively) and the simultaneous net CH_4 production rate (1 fmol cm^{-3} s^{-1} and 5 fmol cm^{-3} s^{-1}, for Lake Tantaré Basin A and Lake Bédard, respectively) indicate that hydrogenotrophy is active in these zones. The negative values of the R_{net}^{DIC} and the fact that the R_{net}^{Ox} = 0 suggest that the rates of the reactions producing DIC, i.e., r1, r2, r5 and r6, can be neglected. The presence of DIC in the Z_3 is likely due to its diffusion from deeper porewater (Fig. 2c and k), but not to its production in the Z_3 through the reactions listed in Table 1. Considering that $R_1 = R_2 = R_5 = R_6 = 0$, the value of R_4 is estimated with Eq. 3 to be 1 fmol cm^{-3} s^{-1} and 5 fmol cm^{-3} s^{-1}, for Lake Tantaré Basin A and Lake Bédard, respectively. Note

that in the Z_3 of Lake Bédard, the net rate value of DIC consumption exceeds by 8 fmol cm^{-3} s^{-1} that of CH_4 production suggesting that DIC is consumed by another process, in addition to hydrogenotrophy. Given that porewater is oversaturated with respect to siderite in that zone (see section 2.4) and that modeling the average Fe concentration profiles with the code PROFILE yields a net Fe consumption rate of −3 fmol cm^{-3} s^{-1} only in that zone (data not shown), we infer that siderite is precipitating at a rate of 8 fmol cm^{-3} s^{-1} in the Z_3 of Lake Bédard, i.e., R_7 = 8 fmol cm^{-3} s^{-1}.

S2.1.3. Modeled $\delta^{13}C$ profiles with the default values

The measured (symbols) $\delta^{13}C$ profiles and those simulated with the default values (purple lines) are displayed in Figure S3. A simulated profile is considered acceptable when it falls within the variability related to the sediment heterogeneity at the sampling sites (grey area fills in Fig. S3). Fig. S3a and b shows that the $\delta^{13}C$ profiles modeled with the default values do not fit adequately the datapoints in both lake basins except for the $\delta^{13}C$-CH_4 profile in Lake Bédard. These discrepancies can be due to inaccuracy of the default f and α_i and in the R_i values, a possibility that is tested below.

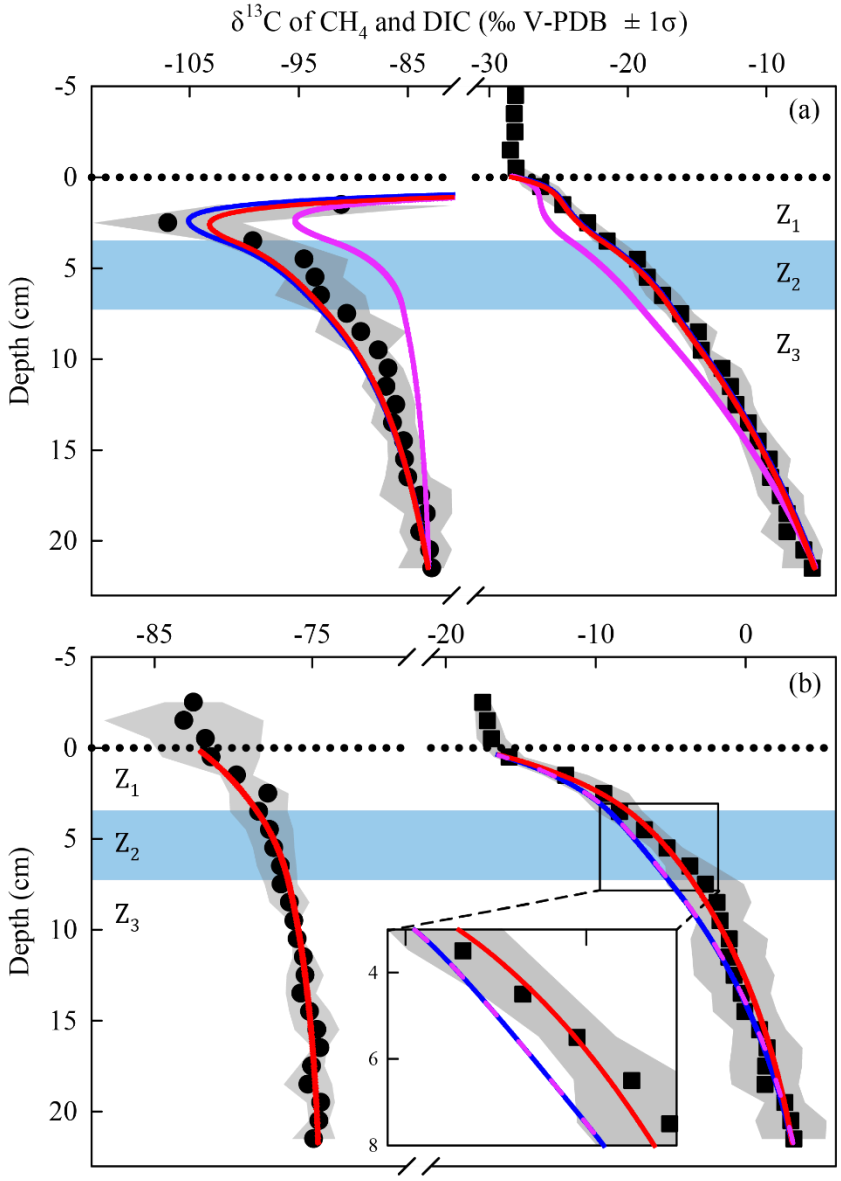

Figure S3: Comparison of the simulated (lines) and measured average (n = 3) $\delta^{13}C$ profiles of CH_4 (circles) and DIC (squares) in the porewater of Lake Tantaré Basin A (a) and Lake Bédard (b). The horizontal dotted line indicates the sediment-water interface. The variability in $\delta^{13}C$ values (± one standard deviation – σ) related to the spatial sediment heterogeneity at the sampling sites is shown by the grey area fills around the data points. The zone Z_2 is delimited by the blue area fill. The purple lines are for the profiles modeled with the default rate and parameter values displayed in tables S1 and S2, the blue lines are for the profiles simulated with the default rate values and optimal α_i and f values as described in section S2.2.1, and the red lines are for the profiles modeled with χ_M = 0.75 (panel a; see section S2.2.2.2 for details) or with α_2 values of 0.980–0.984 in the Z_2 (panel b; see section S2.2.3 for details). Note that the blue and red lines are overlapped for the $\delta^{13}C$-DIC profile in panel a and that the purple, blue and red lines are overlapped for the $\delta^{13}C$-CH_4 profile in panel b.

S2.2. Improving the fit between modeled and measured $\delta^{13}C$ profiles

S2.2.1. Optimizing the α_i and f values

Additional simulations were achieved using in Eq. 7 the default R_i values while varying α_3, α_4, α_5 and f-CH_4 within the range reported in the literature (Table S1) to improve the fits between the modeled and measured $\delta^{13}C$ profiles. Two optimization procedures, based on the minimum N_{res} values, calculated with Eq. 8 for both the $\delta^{13}C$-CH_4 and the $\delta^{13}C$-DIC profiles, were used. One, involved varying sequentially by hand first α_4 and α_3, and then the less influential parameters, i.e., α_5 and f-CH_4 (see Clayer et al., 2018 for details). The other one used a MATLAB® genetic algorithm of the global optimization toolbox, where the algorithm repeatedly provides a population of parameters within the ranges given in Table S1 to perform several hundreds of simulations. At each iteration, the genetic algorithm selects the best performing parameters from the current population and uses them as parents to produce the children parameters for the next generation. Over successive generations, the population of parameters "evolves" toward an optimal solution. The two optimization procedures yielded very similar results and thereafter, we used the MATLAB® genetic algorithm to optimize the parameters and reaction rate values. Note that, during optimization for Lake Tantaré Basin A, α_4 was allowed to take different values in the Z_1, Z_2 and Z_3.

Figure S3 shows that optimizing the f and α_i values greatly improves the fit for Lake Tantaré Basin A only and that the modeled profiles (blue lines in Fig. S3a) capture the main tendencies of the $\delta^{13}C$ profiles measured in this lake basin. Small discrepancies persist between the modeled and measured profiles (e.g., the $\delta^{13}C$-DIC profiles for Lake

Bédard) leaving the possibility that better fits could be reached if more accurate R_i values than the default values were selected.

S2.2.2. Optimizing the R_i values

Uncertainties in the R_i values may result from the assumptions that: i) all the CH_4 was produced by hydrogenotrophy in the sediments of both lake basins (sections S2.1.2.1 and S2.1.2.2), ii) OM oxidation was not a source of DIC in the Z_1 and Z_2 of Lake Tantaré Basin A (section S2.1.2.1 and S2.1.2.2), and iii) the fermenting substrate was glucose in the Z_2 of Lake Bédard (section S2.1.2.2). The mathematical expressions of the R_i have to be modified if we assume that a proportion of methanogenesis occurs via acetoclasty, that a fraction of DIC is produced through OM oxidation, or if the fermenting substrate is more reduced than glucose. The modified expressions for R_i are derived below and summarized in Table S2 for the Z_1 and Z_2 of both lake basins.

Introducing into Eq. 5, the fraction of oxidants consumed by methanotrophy (χ_M) which can take any value between 0 and 1, we can write:

$$R_5 = \frac{1}{2}\chi_M \times (-R_{net}^{Ox}) \quad \text{(S2)}$$

and:

$$R_6 = (1 - \chi_M) \times (-R_{net}^{Ox}) \quad \text{(S3)}$$

Combining Eq. 3 and S2, we obtain:

$$R_3 + R_4 = R_{net}^{CH_4} + \frac{1}{2}\chi_M \times (-R_{net}^{Ox}) \quad \text{(S4)}$$

Introducing into Eq. S4, the fraction of CH_4 produced through hydrogenotrophy (χ_H), we can write:

$$R_4 = \chi_H \left(R_{net}^{CH_4} - \frac{1}{2} \chi_M R_{net}^{Ox} \right) \quad \text{(S5)}$$

and:

$$R_3 = (1 - \chi_H) \left(R_{net}^{CH_4} - \frac{1}{2} \chi_M R_{net}^{Ox} \right) \quad \text{(S6)}$$

By combining Eqs. 3–5, and assuming that $R_7 = 0$, R_1 can be expressed:

$$R_1 = R_{net}^{DIC} - R_{net}^{CH_4} + R_{net}^{Ox} + 2R_4 - R_2 \quad \text{(S7)}$$

Combining Eqs. S5 and S7, we obtain:

$$R_1 = R_{net}^{DIC} - R_{net}^{CH_4} + R_{net}^{Ox} + \chi_H \left(2R_{net}^{CH_4} - \chi_M R_{net}^{Ox} \right) - R_2 \quad \text{(S8)}$$

The expressions for the ranges of the R_1–R_6 values displayed in Table S2, with the notable exception of R_1 in the Z_2 of Lake Bédard, were obtained by substituting into Eqs. S2, S3, S5, S6 and S8 the appropriate values of $R_{net}^{CH_4}$, R_{net}^{DIC} and R_{net}^{Ox} from Table 2. It may be recalled that in deriving these expressions, the following assumptions were made, in accordance with section S2.1.2: i) $R_2 = R_7 = 0$ in the Z_1 and Z_2 of Lake Tantaré Basin A; ii) $R_5 = R_6 = R_7 = 0$ in the Z_1 and Z_2 of Lake Bédard; iii) $R_2 = 0$ in the Z_1 , but not in the Z_2 of Lake Bédard. In order to calculate the values of R_1 with Eq. S8 for the Z_2 of Lake Bédard, we had to express R_1 as a function of the COS of the fermenting substrate as described below.

The rate of H_2 production required through r1 to sustain hydrogenotrophy is given by:

$$\left(\frac{4\nu_1 + y - 2z}{2\nu_1} \right) R_1 = 4R_4 \quad \text{(S9)}$$

Combining Eqs. S5 and S9, we obtain:

$$y = \left(\frac{2\chi_H \left(R_{net}^{CH_4} - \frac{1}{2}\chi_M R_{net}^{Ox} \right) - R_1}{R_1} \right) 4\nu_1 + 2z \quad \text{(S10)}$$

The rate of acetate production through r1 (Table 1) to sustain acetoclasty is given by:

$$\left(\frac{x - \nu_1}{2\nu_1} \right) R_1 = R_3 \quad \text{(S11)}$$

Combining Eqs. S6 and S11, we can write:

$$\nu_1 = \frac{xR_1}{2(1-\chi_H)\left(R_{net}^{CH_4} - \frac{1}{2}\chi_M R_{net}^{Ox} \right) + R_1} \quad \text{(S12)}$$

Replacing ν_1 in Eq. S10 by its expression in Eq. S12, we obtain:

$$y = \left(\frac{2R_1\chi_H \left(R_{net}^{CH_4} - \frac{1}{2}\chi_M R_{net}^{Ox} \right) - {R_1}^2}{2R_1(1-\chi_H)\left(R_{net}^{CH_4} - \frac{1}{2}\chi_M R_{net}^{Ox} \right) + {R_1}^2} \right) 4x + 2z \quad \text{(S13)}$$

The COS of an organic molecule is given by:

$$COS = -\sum_i OS_i \frac{n_i}{n_c} \quad \text{(S14)}$$

where OS_i is the oxidation state of the element *i* and n_i/n_c is its molar ratio to carbon. Assuming that the COS of the fermenting molecule is defined only by H and O atoms, whose OS are respectively +1 and −2, it can be written:

$$COS = -\left(\frac{\left[\left(\frac{2R_1\chi_H \left(R_{net}^{CH_4} - \frac{1}{2}\chi_M R_{net}^{Ox} \right) - {R_1}^2}{2R_1(1-\chi_H)\left(R_{net}^{CH_4} - \frac{1}{2}\chi_M R_{net}^{Ox} \right) + {R_1}^2} \right) 4x + 2z \right] \times (+1) + (z) \times (-2)}{x} \right) \quad \text{(S15)}$$

Eq. S15 can be simplified as:

$$R_1(2COS(1-\chi_H) + 8\chi_H)\left(R_{net}^{CH_4} - \frac{1}{2}\chi_M R_{net}^{Ox} \right) + (COS - 4){R_1}^2 = 0 \quad \text{(S16)}$$

Eq. S16 has two solutions which are $R_1 = 0$, and:

$$R_1 = \frac{(2COS(1-\chi_H) + 8\chi_H)\left(\frac{1}{2}\chi_M R_{net}^{Ox} - R_{net}^{CH_4}\right)}{COS - 4} \quad \text{(S17)}$$

The expression of R_1 for the Z_2 of Lake Bédard given in Table S2 was obtained by substituting into Eq. S17 the appropriate values of $R_{net}^{CH_4}$ and R_{net}^{Ox} from Table 2, and that of R_2 using Eq. S8.

Below, the general expressions of R_1–R_6 displayed in Table S2 for the Z_1 and Z_2 of both lake basins are used to perform additional $\delta^{13}C$ simulations and examine the effect of varying the values of χ_H, χ_M and COS on the modelled $\delta^{13}C$ profiles.

S2.2.2.1. Constraining χ_H the fraction of CH_4 produced through hydrogenotrophy

Figure S4a and b displays the N_{res} values for $\delta^{13}C$ simulations with χ_H comprised between 0.8 and 1 in the Z_1 and Z_2 of both lake basins. Note that the f and α_i values were optimized as described in section S2.2.1 for each χ_H value tested. Whereas, the N_{res} of the $\delta^{13}C$-CH_4 for Lake Tantaré Basin A and Lake Bédard does not vary with χ_H (dotted blue line in Fig. S4a and b), that of the $\delta^{13}C$ -DIC increases significantly as the value of χ_H decreases (dashed blue line in Fig. S4a and b). This finding supports our contention that the contribution of acetoclasty to methanogenesis is negligible in both lake basins, i.e., $\chi_H = 1$ (see section 3.3 and Fig. S2).

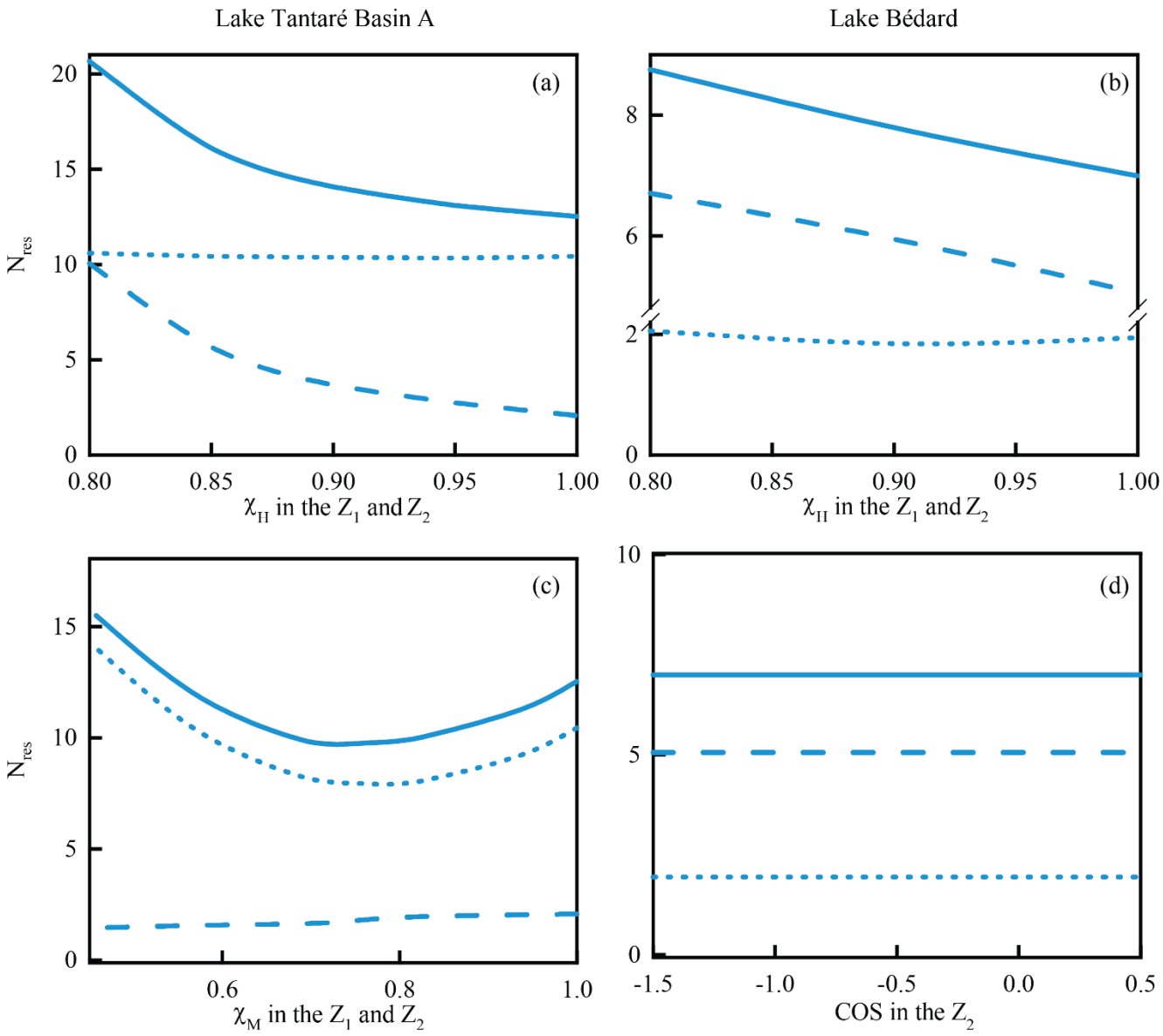

Figure S4: Norm of residuals (N_{res}), calculated with Eq. (8), for the δ^{13}C-DIC (dashed line) and the δ^{13}C-CH_4 (dotted line) profiles, and the sum of N_{res} for the two profiles (solid lines). In panels a and b, the N_{res} values are displayed as a function of χ_H for the Z_1 and Z_2 of both lake basins, in panel c, as a function of χ_M for the Z_1 and Z_2 of Lake Tantaré Basin A, and in panel d, as a function of the COS for the Z_2 of Lake Bédard.

S2.2.2.2. Constraining χ_M the fraction of oxidant consumed through methanotrophy

In section S2.1.2.2, we neglected OM oxidation as a source of DIC in the Z_1 and Z_2 of Lake Tantaré Basin A. Figure S4c shows that the sum of N_{res} for the $\delta^{13}C$-CH_4 and the $\delta^{13}C$-DIC profile displays a minimum at a χ_M value of about 0.75, when χ_M is varied between 0.36 and 1, while maintaining χ_H at 1 and optimizing the f and α_i as in section S2.2.1. Fig S3a (red line) shows that using χ_M = 0.75 in the simulation results in a slightly improved fit of the $\delta^{13}C$-CH_4 profile. This χ_M value implies that about 25% of the oxidant are consumed through OM oxidation in the Z_1 and Z_2 of Lake Tantaré Basin A. Assuming that χ_M = 0.75, we calculate with the equations reported in Table S2 that: R_1 = 132 fmol cm^{-3} s^{-1}, R_4 = 119 fmol cm^{-3} s^{-1}, R_5 = 126 fmol cm^{-3} s^{-1} and R_6 = 84 fmol cm^{-3} s^{-1} in the Z_1 and R_1 = 126 fmol cm^{-3} s^{-1}, R_4 = 78 fmol cm^{-3} s^{-1}, R_5 = 39 fmol cm^{-3} s^{-1} and R_6 = 26 fmol cm^{-3} s^{-1} in the Z_2 (Table 3).

S2.2.2.3. Influence of the COS in the Z_2 of Lake Bédard

Figure S4d shows that varying the value of the COS between −1.5 and +0.5, while maintaining χ_H at 1 and optimizing the f and α_i as in section S2.2.1 has no influence on the modelled $\delta^{13}C$ profiles, i.e., it yields similar N_{res} values. This result was expected given that the COS only affects the values of R_1 and R_2 and that we assumed no fractionation for reactions r1 and r2, as generally proposed in the literature (Lapham et al., 1999; Werth and Kusyakov, 2010; Conrad et al., 2012; Corbet et al., 2015). However, Fig. S3b exhibits a discrepancy between the measured and modeled $\delta^{13}C$-DIC profiles of Lake Bédard. To test if an isotopic fractionation of the DIC assumed to be produced by partial fermentation of HMW OM in the Z_2 of lake Bédard, could explain this discrepancy, we varied α_2 in the simulations. Figure S5 reveals that a minimum N_{res} is

obtained at a value of α_2 = 0.980 for a COS value of 0, as assumed in section S2.1.2.2, and Fig. S3b (red line) shows that using this α_2 value in the simulation results in an improved fit of the δ^{13}C-DIC profile for Lake Bédard. The optimum α_2 value vary slightly with the COS value inferred. For example, for a COS value of −1.5, the optimum α_2 value would be 0.984 (Fig. S5). Varying the COS within reasonable values, however, does not influence significantly the fitting of the δ^{13}C-DIC profile for Lake Bédard shown by the red line in Fig. S3d. Assuming that the COS = −1.5 in the Z_2 of Lake Bédard, we calculate with the equations reported in Table S2 that: R_1 = 72 fmol cm^{-3} s^{-1}, R_2 = 145 fmol cm^{-3} s^{-1} and R_4 = 50 fmol cm^{-3} s^{-1} (Table 3). Note that, considering an α_2 value between 0.980 and 0.984 for the DIC produced through reaction r2 and a δ^{13}C signature of −28‰ for the HMW OM is equivalent to assuming no isotopic fractionation (i.e., α_2 = 0) and a δ^{13}C signature of −8‰ to −12‰ for the source material.

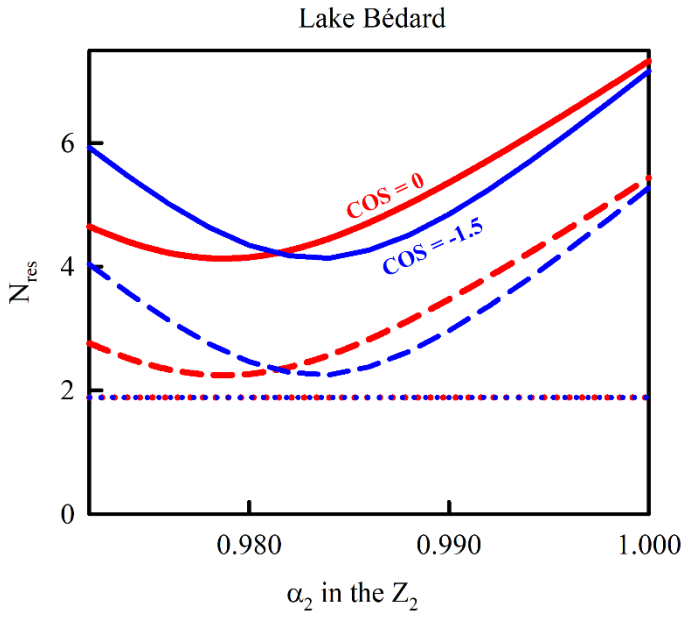

Figure S5: Norm of residuals (N_{res}), calculated with Eq. (8), for the simulated δ^{13}C-DIC (dashed line) and the δ^{13}C-CH_4 (dotted line) profiles, and the sum of N_{res} for the two profiles (solid line) as a function of the value of α_2 in the Z_2 of Lake Bédard.

S3. Other data from Lakes Tantaré, Bédard, Jacks and Lugano used to calculate the COS.

S3.1. Relevant data available and lake characteristics.

Porewater profiles of solutes relevant to the COS calculation, measured by our group in Lakes Tantaré and Bédard at other dates than in the present study, are available from our earlier publications or from our data repository. Profiles of porewater CH_4, DIC, SO_4^{2-}, sulfides (ΣS(−II)) and Fe, determined at the deepest site in the perennially oxic Basin A of Lake Tantaré in September 2004, October 2005, September 2006 and July 2012, have been reported by Clayer et al. (2016). Vertical profiles of the same solutes measured at the deepest site in the sediments of Basin B of Lake Tantaré in October 2006, July 2007, October 2011 and October 2014 can also be found in Clayer et al. (2016 and 2018); the $\delta^{13}C$ profiles of CH_4 and DIC are also provided for the October 2014 campaign (Clayer et al. 2018). Basins A and B of Lake Tantaré, the two westernmost basins of Lake Tantaré, are connected by a shallow channel. This lake is oligotrophic, with a planktonic primary production of 50 mg C m^{-2} d^{-1} measured in Basin A (Hare et al. 1994). Bottom water in Basin B, in contrast to that of Basin A, becomes occasionally anoxic in late summer (Couture et al., 2008). Also, its ^{210}Pb profile reveals no mixing in the uppermost sediment layers and the ^{137}Cs, ^{241}Am and mid-19th century Upper Mississippi Valley Pb isotope chronostratigraphic markers, all display sharp peaks (Gobeil et al., 2013). Collectively, these observations indicate that benthic invertebrates are virtually absent at that site and that solute transport across the sediment-water interface (SWI) should be by molecular diffusion alone. Couture et al. (2010) provide porewater SO_4^{2-}, ΣS(−II)), and Fe profiles determined in June 2004 at the deepest site in

Lake Bédard, and an unpublished set of porewater profiles of CH_4, DIC, SO_4^{2-}, ΣS(−II) and Fe obtained in October 2003 by our group with the methods described by Clayer et al. (2016) is also available from our archives. The profiles of ^{210}Pb, ^{137}Cs, and stable Pb isotope (Gobeil et al., 2013) all point out to the absence of benthic invertebrates in Lake Bédard sediments.

Carignan and Lean (1991) reported porewater DIC, CH_4, NH_4, ΣS(−II), P, Si, Fe, Mn, Ca, Mg, K and pH profiles obtained in September 1981 with peepers at 5 sites of varying depth (4, 10, 15, 20.2 and 21.7 m) along a transect in the Williams Bay of Jacks Lake (44º41' N, 78º02' W). This lake is located ~65 km north of Peterborough, Ontario, on the fringe of the Canadian Shield and the bedrock of its forested watershed comprises mainly felsic rocks with minor limestone outcroppings (Pick et al., 1984). The dimictic Williams Bay is mesotrophic, with a ^{14}C primary production of ~900 mg C m^{-2} d^{-1}, and it develops an anoxic hypolimnion from mid-June to September. The presence of ΣS(−II) in the water overlying the sediments indicates anoxia at the sediment surface of all stations in September. Carignan and Lean (1991) mention that macrobenthos activity at the two shallowest stations should be suspected from the ^{210}Pb and the DIC and CH_4 profiles, and that a loss of CH_4 may have occurred during retrieval and sampling of the peepers and have altered the lower part (below ~30 cm) of the CH_4 profiles at the three deepest stations. The authors identified by SEM/EDAX solid Fe sulfide particles ($FeS_{2(s)}$ and $FeS_{(s)}$) in the sediments of the three deepest stations but were unable to detect carbonates ($FeCO_{3(s)}$ or $CaCO_{3(s)}$).

Porewater profiles of CH_4, DIC, Ca, Fe, SO_4^{2-} and ΣS(−II) have been obtained with peepers (Lazzaretti et al., 1992; Lazzaretti-Ulmer and Hanselmann, 1999) in June

1989, September 1989 and March 1990 at two sites (Melide, 85 m depth and Figino, 95 m depth) located in the southern basin of Lake Lugano (46°00'N; 03°30'E; Switzerland). This lake basin is monomictic, with the overturn occurring in February. It was originally oligotrophic but it had become eutrophic in 1989 for more than 30 years due to increasing nutrient loads, and it showed a primary production rate of up to ~1260 mg C m^{-2} d^{-1} (Barberi and Mosello, 1992; Niessen et al., 1992). As shown in the papers by Lazzaretti et al. (1992) and Lazzaretti-Ulmer and Hanselmann (1999), the redox conditions at the SWI varied markedly with time. In the overlying water, in March 1990, [O_2] concentration was ~2 and 4 mg L^{-1} at the Figino and Melide sites, respectively, and ΣS(−II), CH_4, Fe(II) and Mn(II) were absent in the lake bottom water, supporting oxidizing conditions at the SWI at the two sites at that date. In contrast, in June and September 1989, the SWI at the two sites was anoxic since ΣS(−II), CH_4, Fe(II) and Mn(II) were present in the overlying water (except Fe in June at the Figino site). The sediments at the two sites are characterized by the presence of carbonate and clay varves (Span et al., 1992) and by the absence of benthos remains in the pre-1970 layers (Niessen et al., 1992), indicating the absence on benthic animals.

S.3.2. Data treatment

The relevant porewater profiles for Lake Bédard and for the two basins of Lake Tantaré were gathered from our archives or from our earlier publications. For Williams Bay of Jacks Lake and for Lake Lugano, the published plots of the porewater solutes of interest were enlarged electronically, and the coordinates of the data points were determined to reconstruct the solute concentration vs depth profiles. The measured CH_4 and DIC profiles for Lakes Tantaré, Bédard, Jacks (Williams Bay) and Lugano along

with their respective modeled profiles using the code PROFILE are displayed in Fig. 4. For Williams Bay, only the profiles reported at 15 m and 22 m were retained in this study; those from the two shallowest sites (4 m and 10 m) were ignored because of sediment bioirrigation (Carignan and Lean 1991), whereas those from the 20-m site were discarded because modeling with PROFILE predicted an extremely low net DIC production rate. For Lake Lugano, the data pertaining to March 1990 and June 1989 were kept; those reported for September 1989 were rejected because the CH_4 and DIC concentration profiles were almost linear and modeling with PROFILE did not show any zone of significant net CH_4 production. The R_{net}^{Ox} values were calculated, as described in section 2.3, from the consumption rates of the electron acceptors (EAs; O_2, Mn(IV), Fe(III) and SO_4^{2-}) obtained by modeling the porewater depth distributions of O_2, Mn(II), Fe(II) and SO_4^{2-} with the code PROFILE. To estimate the contribution of the O_2 consumption rate to R_{net}^{Ox} in March at the two sites of Lake Lugano, we assumed that the $[O_2]$ at the sediment surface was 2 $mg.L^{-1}$ at Figino and 4 $mg.L^{-1}$ at Mélide, i.e., the concentrations measured in the water column, near the sediment surface at these sites (Lazzaretti et al, 1992). The absence of sulfate data for Williams Bay prevented us from calculating R_{net}^{Ox}. The production rate of DIC due to carbonate dissolution in the porewaters was calculated by modeling with PROFILE the porewater Ca profiles for the two sites in Lake Lugano, and its contribution was removed from the R_{net}^{DIC}; this calculation was unnecessary for Williams Bay where this dissolution reaction did not occur. In modeling with PROFILE, we assumed that $\alpha_{irrigation}$ was negligible, even in March for the two sites at Lake Lugano, given the evidence that macrobenthos is absent. Note that the R_{net}^{DIC} and R_{net}^{Ox}values are weighed average values calculated over a zone of net methanogenesis. The $R_{net}^{CH_4}$, R_{net}^{DIC} and R_{net}^{Ox} values are regrouped in Table 4 for the various lake basins.